Design of Antennas from Primitive Shapes Using Genetic Algorithms

Julie Rolla,* **Bryan Reynolds,†** **Dylan Wells,†** **Jacob Weiler,†** **Amy Connolly,†** **and Ryan Debolt†**

ABSTRACT. — This report presents developments to a genetic algorithm that evolves antenna designs from primitive shapes. The gain patterns of individuals are evaluated using XFdtd electromagnetic simulation software, and fitness is evaluated by comparison to a target gain pattern. This work is an update to a prior report demonstrating evolution of 3D structures to target geometries. The algorithm was updated to evolve antennas by adding feeds, early shorting prevention, and simulation components. Different fitness functions were developed, and differences in convergence to similar gain patterns was explored. Computational efficiency was also improved by converting to an asynchronous steady-state algorithm and incorporating, among other improvements, an elite method, and a diversity forcing feature. The algorithm was able to evolve antennas to match the desired gain pattern using each fitness function. The algorithm was run for a single-frequency (300 MHz) design and for a broadband case (200 MHz to 800 MHz). Later versions of the algorithm will utilize fitness functions connected to science simulation software to generate designs optimized to science outcomes. Future improvements to the algorithm to facilitate more complex designs and to reduce computation time are also discussed.

I. Introduction

This report introduces an evolutionary algorithm that evolves antennas from primitive shapes to specified gain patterns *without* predefined antenna topologies (i.e., dipole or biconical). It expands upon the previous August 2023 Interplanetary Network Progress Report "Design of 3D Antenna Geometries Using Genetic Algorithms,"

*Tracking System and Applications Section.

†Department of Physics, Center for Cosmology and AstroParticle Physics, The Ohio State University.

The research described in this publication was carried out by the Jet Propulsion Laboratory, California Institute of Technology, under a contract with the National Aeronautics and Space Administration.

where a method for evolving 3D structures using genetic algorithms (GAs) was developed [1]. The initial report demonstrated an algorithm capable of creating 3D structures that matched predefined target shapes, marking an initial step toward the goal of designing optimized antennas for specific scientific outcomes. The method consisted of assembling geometric primitives and evaluating fitness using cost functions tied to the design's similarity to a target shape. This work builds on the previous GA by implementing cost functions that are derived from performance metrics based on antenna radiation patterns produced in XFdtd, an electromagnetic finite difference in the time domain simulation software by Remcom [2]. Individuals are evaluated on their similarity to a predefined target gain pattern or sensitivity in specified directions. Additionally, several enhancements to the previous GA were made to improve the speed of converging to a high-quality solution and consequently reduce computation time. Future versions of the algorithm will evolve toward complex science goals by integrating experiment simulation software and broadening its capabilities to generate antennas with more complex designs.

This work was originally motivated by astrophysics experiments dependent on highly sensitive detectors, although the potential impact goes beyond astrophysics by reducing instrument development overhead while adhering to constraint considerations. The design of such instruments poses a substantial challenge, especially when restricted by scheduling and cost limitations. These optimization tasks typically occur in high-dimensional parameter spaces with multiple objectives and are computationally prohibitive to solve using traditional techniques; however, using innovative Artificial Intelligence (AI) optimization algorithms, such as GAs, vast parameter spaces can be realistically explored. This report delves into utilizing GAs to design antennas optimized for specific antenna responses, with future goals of multiobjective optimization tied to sensitivity to science outcomes. GAs are computational heuristics that mimic evolutionary principles to efficiently identify solutions to defined problems. Although this endeavor has the potential to expand to a wide range of detector technologies, the immediate focus is on enhancing sensitivity for radio observations, including antennas for the Global Navigation Satellite System (GNSS) [3, 4, 5], passive sounding [6, 7, 8], and low-frequency astronomy radio signals, including radio emissions from extrasolar planets [9, 10, 11], cosmic ray electrons and cosmic magnetic fields [12, 13, 14, 15, 16], and the highly redshifted neutral hydrogen hyperfine line [17, 18, 19, 20]. By addressing a critical need for innovative early-stage design optimization tools, this work aims to increase the scientific capabilities of future astrophysics experiments (ranging from instrumentation on flagship missions to low-cost SmallSats), which face complex performance, geometry, and budget requirements.

Evolutionary algorithms have been used in a variety of applications, including antenna design, and remain a focal point of active research [21, 22, 23, 24]. Antenna array optimization using GAs has also been an area of recent development [25, 26, 27]. The Genetically Evolving Neutrino Telescopes (GENETIS) collaboration has pioneered the

integration of GAs with antenna and science simulation software, aiming to design biconical and horn antennas with improved sensitivity to neutrino signals [28, 29, 30, 31, 32]. McCarthy et al. utilized a GA to design a horn antenna for detecting of Cosmic Microwave Background radiation [33]. Furthermore, the Long-Baseline Neutrino Oscillation (LBNO) experiment and the Deep Underground Neutrino Experiment (DUNE) optimized the design of neutrino beamlines through a GA using science simulations to determine fitness [34, 35]. GAs have contributed to optimizing various aspects of detector design, including layout, sensors, shielding, trigger optimization, and antenna arrays [36, 37, 38, 39, 40].

GAs are a powerful heuristic search method capable of finding high-quality solutions to complex problems [41, 42, 43, 21]. They are effective in problems with many high-cardinality parameters and have been successfully demonstrated in numerous applications across many disciplines. Rooted in principles of biological evolution, GAs begin with an initial set (population) of solutions (individuals) that undergo iterative evolution toward improved results. Individuals are evaluated by a cost or fitness function, which informs the selection of parents (using techniques called selection methods) for the generation's new designs, called children. Children are formed from parents with various methods of mutating or combining individuals through techniques called operators. As in biology, evolutionary pressure induced by selection methods tied to cost functions results in individuals with enhanced designs. Given their stochastic nature, GA results will fluctuate when evolving toward the same solution multiple times. To increase the probability of a successful algorithm, consideration must be taken in the design of selection methods, genetic operators, hyperparameters, and, most importantly, the fitness function.

Expanding to build antennas, instead of simple 3D structures shown in our previous report, required three main developments to the GA. First, the construction of 3D models transitioned to utilize XFdtd in order to simulate the individual gain patterns required by the fitness calculations, moving away from Blender [44], an open-source 3D modeling software. Second, adjustments were made to the structures to include the antenna feed and ground components that are necessary to generate an antenna response. Finally, mechanisms were established to prevent the designs from shorting across the feed and ground points, as such designs are typically ineffective. These modifications and the associated challenges are discussed in more detail in Section II.B.

This report presents initial findings resulting from the use of a GA to construct antennas and evolve individuals optimized for desired antenna responses. Section II describes a detailed overview of the GA, including constructing an individual, XFdtd simulations, fitness evaluation, and the selection methods and operators. Section III, describes the process of calculating various fitness scores that were explored. The results of the evolution using each fitness function are given in Section IV. Finally, Section V discusses the significance of the results, the next steps in evolving antenna designs toward specified science outcomes, and identifies potential challenges.

II. Genetic Algorithm

A flowchart of the GA used in this analysis is shown in Figure 1, and the steps are discussed in detail in this section. The loop begins by generating an initial population of solutions. Following the steps described in Section II.A below, the algorithm generates individuals and then constructs those designs in XFdtd. XFdtd simulates the gain response pattern of each individual, which allows fitness scores to be calculated by comparing each response pattern to a target gain pattern. The fitness scores are then used to select parents and create offspring. The GA has a numerous parameters outlined in Appendix I.

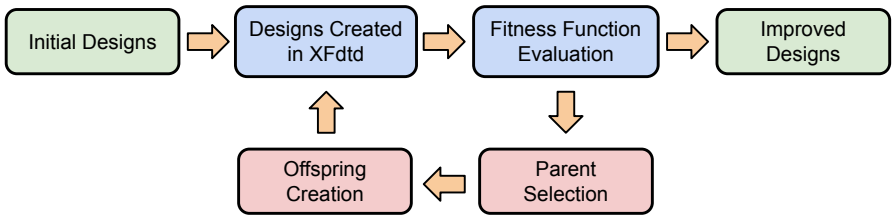

Figure 1. Diagram illustrating the basic loop of the GA. Green boxes indicate initialization and termination. The blue boxes show the steps required to evaluate the fitness function, and the red boxes give the steps for creating the new individuals.

A. Building an Individual

Single individuals are built from basic geometric primitive shapes connected to form a more complex structure as shown by the example on the left side of Figure 2. Future iterations of the algorithm will allow for disconnected components that affect the antenna beam pattern, such as reflectors and directors used in Yagi-Uda antennas. These primitives may be thought of as building blocks taking the form of one of four primitive shapes: cuboids, cylinders, cones, or spheres. An individual is fully described by the dimensions, location, orientation, and connections of each component shape. In the code, an individual is represented by a dictionary tree structure that contains the genes of all the component shapes. The right side of Figure 2 illustrates the tree structure for the example individual. Currently, each side of a shape is only allowed to have one connected shape. All shape types behave consistently, with a maximum of one attachment allowed in each region corresponding to its front, back, left, right, top, and bottom. Additionally, when cylinders and cones are added to another shape, they always connect with their flat top or bottom face. In this analysis, individuals were allowed to be constructed with up to seven primitive shapes. A more thorough discussion of the basic methodology for individual construction is given in the prior progress report [1].

For the constructed geometries to perform as antenna designs, several additions were implemented, including the placement of voltage feed and ground points and the prevention of unwanted shorting across the feed point. The algorithm begins constructing an individual by first creating a small cube at the origin as a placeholder

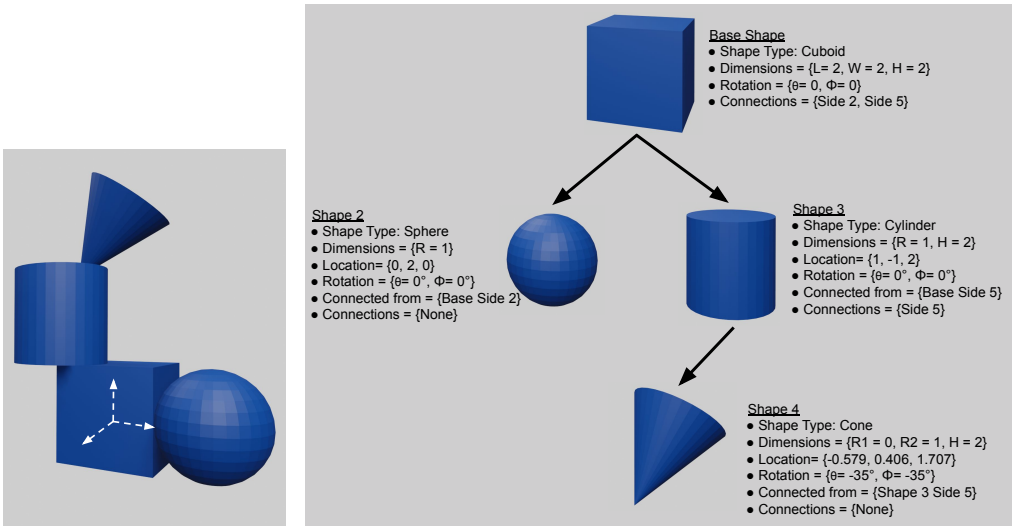

Figure 2. Left: Example individual consisting of each of the four primitive shapes. A base cuboid at the origin with an attached cylinder and sphere. The cylinder then has an attached cone. Right: Tree structure of example individual, with the genes of each shape listed.

for the antenna feed and ground assemblies and then builds off of it with new primitives. In its current state, the algorithm is designed to focus on the construction of single-feed dipole-shaped antennas. As such, it is required that exactly two primitives be placed on separate sides of the starting cube in all evolved designs, with one primitive to be attached to the antenna feed line and the other to the ground.

To prevent potential antenna performance issues caused by shorting across the feed point, a collision detection algorithm utilizing the open-source Flexible Collision Library software package was implemented [45]. In this algorithm, a bounding volume is created that encloses each primitive that makes up an individual. Each time a new primitive is added or the genes of an existing primitive are changed, the algorithm disallows any operations that cause overlap between primitives that are electrically connected to opposite sides of the feed point. It is acknowledged that universally disallowing shorting limits the potential antenna designs that the algorithm may create; however, this is suitable for the single-feed dipole-like cases that are the focus of this report. Future work will incorporate more complex logic to allow for designs where the feed and ground are electrically connected, such as loop dipoles or some log-periodic dipole arrays.

B. Creating Antennas in XF

Once the tree describing an individual is created as a dictionary, it is converted to a model in XFdtd through the program's scripting API. The algorithm allows for the material properties of the antenna designs to be evolved; however, all studies presented in this report defined the primitives to be hollow and made from perfect electrical conductor material. Before XFdtd simulation and fitness evaluation, the

starting cube is removed and replaced with the antenna feed. The algorithm allows for single-frequency or broadband-frequency designs. For this work, the single-frequency runs simulated the response at 300 MHz, while the broadband runs used 37 different frequencies of equal steps from 200 MHz to 800 MHz. The antenna response was simulated at 5° increments of the azimuth-zenith coordinates. The increment size can be adjusted as needed for specific applications. The gain of an antenna is a measure of how efficiently it converts received radio waves from a given direction into power. XFdtd calculates the far-zone realized gain (hereafter referred to as simply "gain") of an antenna at a specific (θ, ϕ) coordinate using Eq. 1 [46]:

$$G_{\mathrm{R}} \;=\; \frac{2\pi r^2 |\widetilde{E}(\theta,\phi)|^2}{\eta P_{\mathrm{M}}} \;. \tag{1}$$

Here, G_{R} is the realized gain [47] of the antenna in a specific direction in dBi. $\widetilde{E}(\theta, \phi)$ is the complex electric field incident on the antenna from the (θ, ϕ) direction, η is the wave impedance in the medium (377 Ω in free space), r is the distance between the power source and the sensors in the simulation (1 m), and P_M is the power accepted by the antenna. The gain is equivalent to the directivity multiplied by the antenna's radiation efficiency.

C. Fitness Function Calculation

Once an individual is simulated in XFdtd, fitness functions are used to compare the resulting gain pattern to the desired goal. Two fitness functions were developed and tested during this analysis: Euclidean distance and directional gain, which are described in detail in Section III.

D. Parent Selection

This analysis used tournament selection as the sole selection method. In tournament selection, a small subset of the population is chosen at random, and the individual with the highest fitness score in the subset is selected as a parent [48, 49, 50, 51]. We used a tournament size of 7% of the population or 8 individuals for a population of 120.

E. Genetic Operators

This section describes the three main genetic operators that were used to build the next generation: mutation, crossover, and injection.

Mutation alters one component of a single parent individual to produce an offspring. Due to the complexity of combining shapes into individuals, two different types of mutation were implemented: standard mutation, where a single gene is altered, and regenerative mutation, where an entire component shape is altered. In standard mutation, a single dimension, rotation, or location gene of a single shape is altered by

generating a value from a Gaussian distribution centered on the original value, where the standard deviation is a predefined percentage of the total range of values. While standard mutation makes minor changes to individuals, regenerative mutation allows larger changes to occur. There are four types of regenerative mutation: grow, prune, replacement, and side switch. For grow mutation, an empty side of one shape on the individual is selected, and a new shape is generated that connects to that side. In prune mutation, a shape, and all subsequent connected shapes in the tree, are removed from the individual. Replacement mutation is the process of exchanging one shape with another, where the new shape is generated from scratch. During the evolutions tested in this work, we noticed that some plateaus were the result of a replacement mutation that rarely performed well, as the new shape would often have geometry very different from the previous shape. For example, a dipole that approximates a cone with similar dimensions will perform better than a cone with a very different geometry. To ameliorate this, a proportional replacement mutation was developed and added to the algorithm during the broadband runs, which causes the new shape to have dimensions that are similar to the shape it is replacing. Finally, side switch mutation selects a shape and moves it, and all subsequent connected shapes in the tree, to a different unoccupied surface of the shape to which it was originally connected.

Components of two parents are combined to produce two offspring in gene or branch crossover. In gene crossover, two parents exchange a single gene of one shape. The shapes are restricted to be the same type, unless the gene swapped is rotation or location. In branch crossover, all shapes in one branch of the tree structure are swapped between the two parents. The algorithm selects a tree depth in each of the parents and then exchanges the branches off that point. The branch to swap from a parent is allowed to be empty, which would effectively trim the branch of the other parents. As with mutation, the algorithm ensures that the shape is still valid and that the constraints are still satisfied.

Injection is the creation of a brand new individual in the next generation. Individuals made by injection are created using the same method as individuals in the first generation.

F. Steady-state Evolution

In an improvement to the prior algorithm, this version incorporates an asynchronous steady-state methodology, where new children are immediately introduced into the population, instead of having delineated generations [52, 53, 54, 21]. After the initial population is evaluated, a single new child is created where the type of genetic operator used is chosen based on a predefined probability. Once the child is created, a random individual in the population is replaced by the new child. This increases evolutionary pressure by allowing the genetic information from a child to be immediately available for the population, which reduces computation time by increasing the rate of convergence. For comparison with traditional GAs, we define that a new generation

occurs when new children equal to the population have been created.

Two additional features were added to complement the change to steady-state evolution. First, we implemented an elitism constraint, where the individual with the highest fitness is always preserved, meaning that it cannot be removed from the population. This feature replaced the reproduction operator, used in the previously reported algorithm, that directly copied a parent to the next generation. Second, a forced diversity feature was implemented during individual construction, which requires that there are no duplicate individuals in the population. Prior to implementing these changes, initial tests of the steady-state algorithm resulted in large numbers of duplicate individuals and large plateaus that the GA was not able to break out of due to a lack of diversity in the population.

III. Fitness Function Details

This section details the Euclidean distance and directional gain fitness functions that were developed for the purposes of this algorithm.

A. Euclidean Distance Fitness Function

The Euclidean distance is used as a metric to determine the similarity between N-dimensional vectors by summing in quadrature the corresponding elements of each vector. A Euclidean distance of zero indicates perfect matching between vectors, and larger values indicate a greater degree of dissimilarity. The general form for Euclidean distance between vectors n and m, where i is the Nth component is given by Equation 2:

$$d(\vec{n}, \vec{m}) = \sqrt{\sum_{i=1}^{N} (n_i - m_i)^2} \tag{2}$$

To compare an individual's simulated radiation pattern to the target, complex values that encode the gain and phase in each sampled direction are calculated in the vertical, v, and horizontal, h, polarizations separately, as shown in Equations 3 and 4.

$$Z_v = G_v \left[\cos(\Phi_v) + i \sin(\Phi_v)\right] \tag{3}$$

$$Z_h = G_h \left[\cos(\Phi_h) + i \sin(\Phi_h)\right] \tag{4}$$

G_v and G_h represent the gain in each polarization direction, and Φ_v and Φ_h represent the phase in each polarization direction.

This complex value is evaluated at each point, i, sampled in θ and ϕ for both the evolved and target antenna gain patterns, and, accounting for the vertical and

horizontal polarizations independently and weighting their contributions, the Euclidean distance-based fitness metric comparing the resulting vectors takes the form shown in Equation 5.

$$d = \sqrt{\left(\sum_{i=1}^{N}\left[A\left|Z_{v_i,\text{evolved}} - Z_{v_i,\text{target}}\right|^2 + B\left|Z_{h_i,\text{evolved}} - Z_{h_i,\text{target}}\right|^2\right]\right)} \tag{5}$$

Here, the weights of the contributions from each polarization are represented by A and B, which are constrained to obey the relationship $A + B = 1$. For all studies presented in this report, each polarization was given equal weighting, leading to $A = B = 0.5$ This metric is the basis for the Euclidean distance fitness function given by Equation 6.

$$F_E = \frac{1}{1+d} \tag{6}$$

Fitness scores resulting from the Euclidean distance-based metric are bound between $F_E = 0$ and $F_E = 1$. Scores approaching 1 correspond to evolved antenna designs with radiation patterns exhibiting a high degree of similarity with the target radiation pattern. A fitness score of 1 indicates that the evolved antenna's radiation pattern and phase perfectly match that of the target.

1. Single-frequency and Broadband Applications

The Euclidean distance fitness function maintains the form presented in Equations 5 and 6 when used to evaluate the similarity between the radiation pattern of an evolved antenna with that of the target for both single-frequency and broadband cases. The broadband case requires that the gain and phase values at all sampled points in the simulated radiation patterns corresponding to each frequency step in the user-defined band be considered in the fitness score calculation. The single-frequency case simply considers one radiation pattern at a single specified frequency to derive the fitness score.

B. Directional Gain Fitness Function

A fitness function was devised to maximize and/or minimize gain in user-specified angular ranges, directing antenna designs to evolve toward an optimal directional sensitivity profile. This required separate contributions to the fitness score accounting for gain values in the angular ranges to be maximized, where larger values must positively impact the fitness score, and gain values in angular ranges to be minimized, where larger values must negatively impact the fitness score. The highest scoring individuals will have the highest average gain in maximization regions and lowest average gain in minimization regions. An equation was then created to meet these desired outcomes, which gives the directional gain fitness function, F_D, in Equation 7.

$$F_D = A\left[\tanh\left(\bar{G}(\theta_{max}, \phi_{max})\right)\right] + B\left[\frac{1}{1 + \bar{G}(\theta_{min}, \phi_{min})}\right] \tag{7}$$

Where $\bar{G}(\theta, \phi)$ represents the average gain over all sampled points in the user-specified angular ranges for the sensitivity to be maximized or minimized, which is denoted by θ_{max} and ϕ_{max}, and θ_{min} and ϕ_{min}, respectively. The first term accounts for the maximizing range and is weighted by A, while the second term describes the minimizing range and is weighted by B. The weights are constrained to $A + B = 1$. For all studies using this fitness function in this report, the two terms were evenly weighted, with $A = B = 0.5$. This means that maximizing and minimizing gain in the respective angular regions of interest is given equal importance in the determination of this metric of fitness.

This fitness function was designed to be bounded between 0 and 1. However, it is worth noting that to achieve a fitness score of 1, an infinite gain would be required in the region where gain is to be maximized, which is not possible for physical antennas. High-performing individuals in the studies presented in Section IV.B of this report achieved fitness scores nearing 0.9 under this metric.

1. Single-frequency and Broadband Applications

The directional gain fitness function maintains the form presented in Equation 7 applied to both single-frequency and broadband cases. The difference between these cases lies in the calculation of the average gain at points in the angular range(s) where maximization or minimization is desired, $\bar{G}(\theta_{max}, \phi_{max})$ and $\bar{G}(\theta_{min}, \phi_{min})$, respectively. The average gain calculations for the single-frequency case consider gain values in the specified angular ranges from the simulated antenna radiation pattern at a single specified frequency. The average gain calculations for the broadband case account for gain values in the specified angular ranges from the simulated antenna radiation patterns at each frequency step in the user-specified band. At present, contributions from the gain at each sampled point in the specified ranges of maximization and/or minimization, from all frequency steps in the band, are given equal weight in the calculation of $\bar{G}(\theta_{max}, \phi_{max})$ and $\bar{G}(\theta_{min}, \phi_{min})$. However, future implementation to allow for increased importance to be placed on performance at specific in-band frequencies is planned.

IV. Results and Discussion

The GA was tested using both the Euclidean distance and the directional gain fitness function. For each fitness function, designs were evolved once for a single frequency of 300 MHz and once for a broadband case of 200 MHz to 800 MHz. For the broadband case, the simulated antenna radiation patterns are evaluated at 37 evenly spaced discrete frequency steps in the specified band. This section describes the details of the

evolutions for each of the four tests. For each evolution discussed in this section, the population size was 120 individuals.

A. Euclidean Distance Target Radiation Pattern Evolution

1. Single Frequency

Figure 3 shows the results for the Euclidean distance evolution at a single frequency of 300 MHz. The single-frequency target radiation pattern is that of a simple dipole. The highest fitness score of each generation is plotted as the solid green line and quartiles are shown as the other lines. Over 441 generations, the designs evolved to a fitness score of approximately 0.75. The 3D models corresponding to the most fit individuals (red) as of generations 0, 25, and 441 are shown in comparison to the model (blue) that created the target radiation pattern in Figure 4.

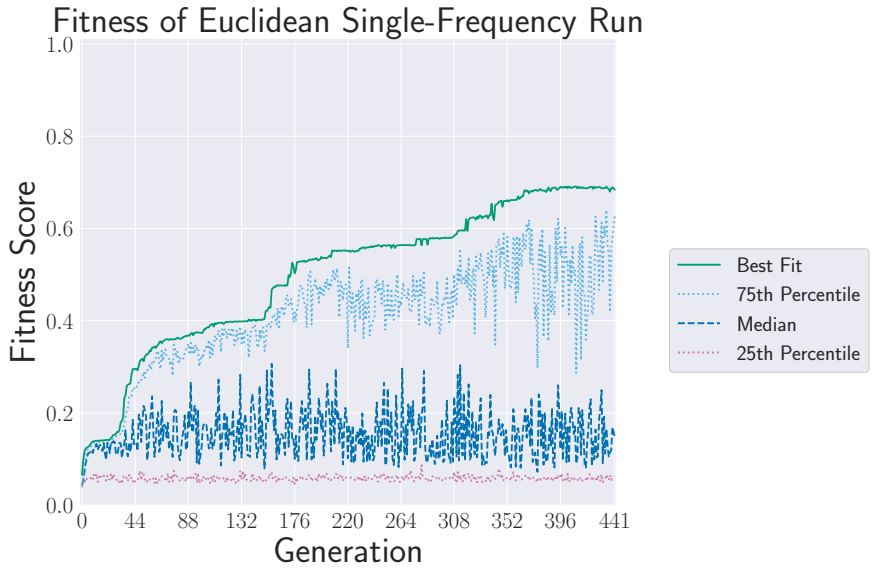

Figure 3. The fitness score of each generation evolving toward a single-frequency radiation pattern using the Euclidean distance fitness function. The maximum fitness score and the three quartiles are shown.

Figure 5 shows the gain patterns of the most and least fit individuals, represented by the green and blue lines, respectively, at the start and end of the evolution, along with the target gain pattern for reference, represented by the pink diamonds. Here, the gain patterns are represented as two-dimensional slices in the zenith and azimuth directions. Images of the full three-dimensional gain patterns corresponding to these slices may be seen in Figure 19 in Appendix II. Figure 6 depicts the phase, in the zenith and azimuth directions, of the most and least fit evolved antennas at the beginning and end of the evolution. The phase of the most and least fit individuals is represented by the green and blue lines, respectively, while the phase of the target is shown in pink. Additional gain and phase results of the most and least fit individuals

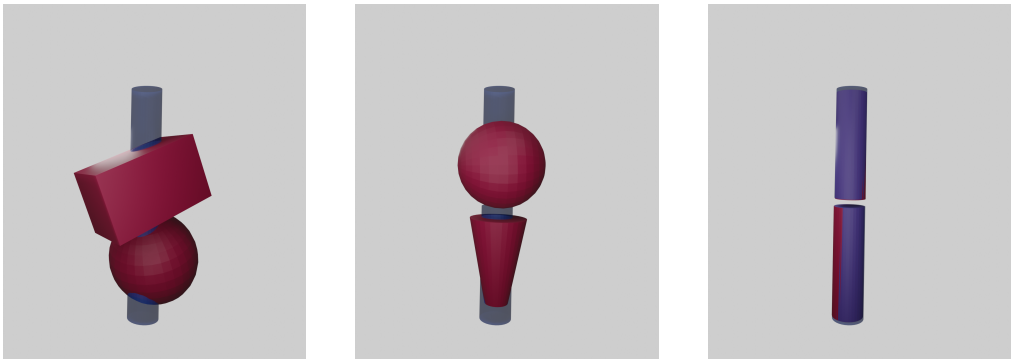

(a) Generation 0 (b) Generation 25 (c) Generation 441

Figure 4. Three example models of the best individual of generations 0, 25, and 441 are shown, illustrating the evolution of the antenna using the Euclidean distance fitness function. The antenna that produced the target gain pattern is given in blue, and the individual is shown in red.

at an intermediate generation are displayed in Figures 27 and 28 in Appendix III.

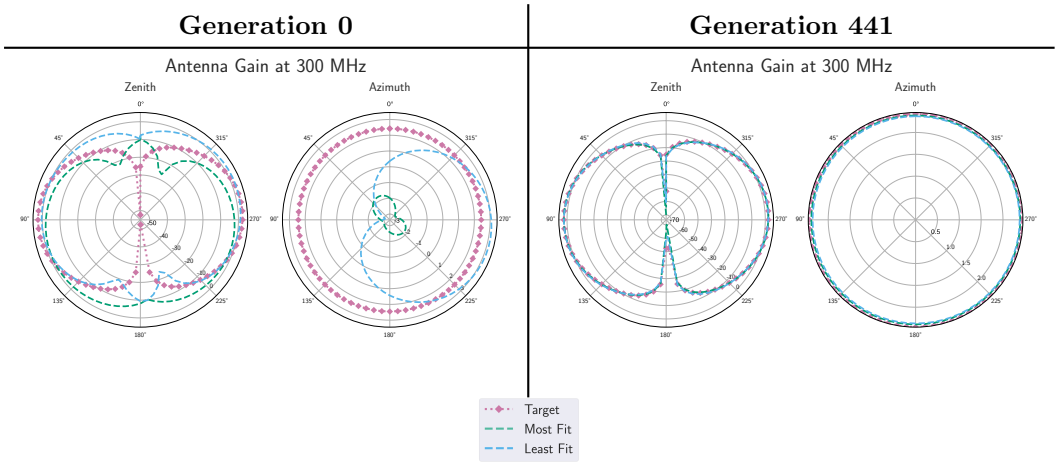

Figure 5. The gain patterns of the most and least fit individual as of generations 0 (left) and 441 (right) of the single-frequency evolution towards a target radiation pattern using the Euclidean distance fitness function. Also overlaid on each is the gain pattern of the target.

Despite the fitness score peaks at approximately 0.7, Figure 5 shows that the most fit individual has a gain pattern that is closely aligned with the target. The difference between the evolved antenna's performance and that of the target lies almost entirely in the antenna phase near 0° as measured in the zenith direction, as evidenced in Figure 6. This illustrates that a single data point can have a large effect on the fitness score of an individual.

2. Broadband Target Radiation Pattern Evolution

The broadband target radiation patterns consisted of antenna gain and phase evaluated at 37 discrete, evenly-spaced frequency steps between 200 MHz and

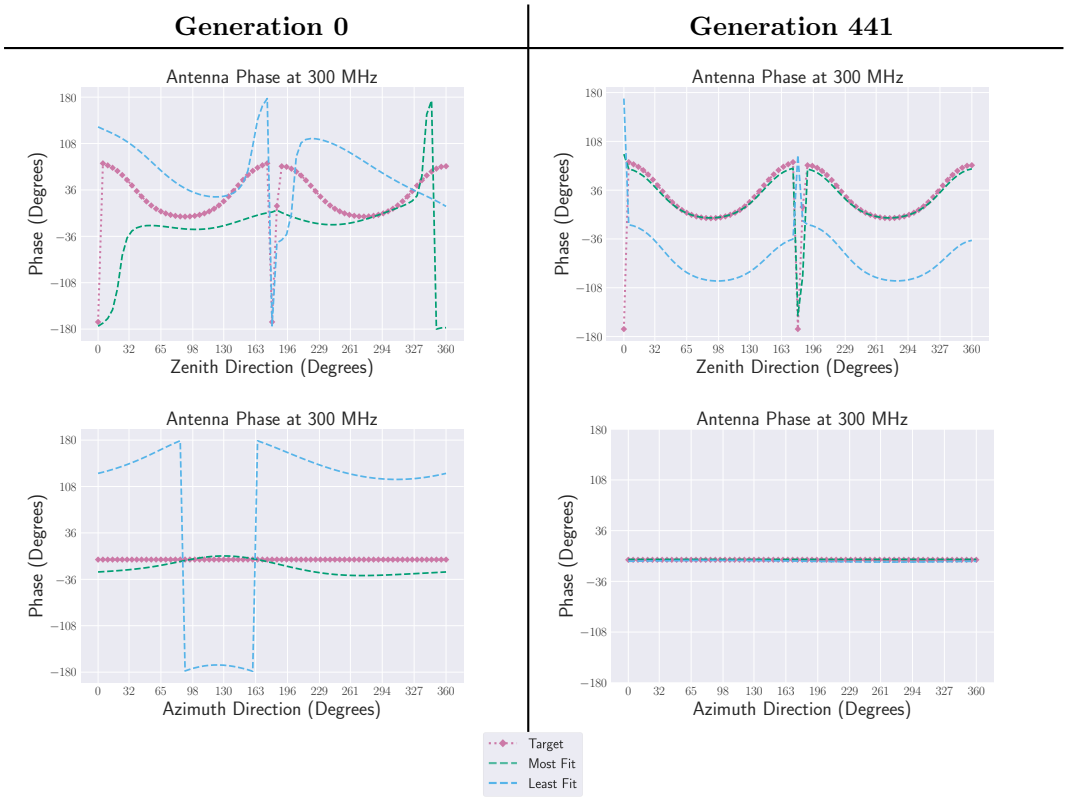

Figure 6. The antenna phase in the zenith and azimuth directions of the most and least fit individual as of generations 0 (left) and 441 (right) of the single-frequency evolution towards a target radiation pattern using the Euclidean distance-based fitness function. Also overlaid on each is the phase of the target.

800 MHz. The radiation patterns chosen as targets for the broadband evolution towards a target test case corresponded to the designs of broadband antenna created through the GENETIS collaboration's studies on optimization of the biconical antenna designs [28]. Figure 7 shows the results for the Euclidean distance evolution for the broadband case. Here, the highest fitness score of each generation is plotted as the solid green line and quartiles are shown as the other lines. After 216 generations, the most fit individual created in the evolution achieved a fitness score of approximately 0.39. The models corresponding to the most fit individuals as of generations 0, 5, and 216 are shown overlaid with the model corresponding to the target radiation pattern in Figure 8.

Figure 9 shows the most and least fit individuals, represented by the green and blue lines, respectively, at the start and end of the evolution at three example frequencies of 200 MHz, 516.73 MHz, and 800.01 MHz, representing the upper, lower, and middle frequencies in the band. The target gain pattern at each frequency is also shown for reference and is represented by the pink diamonds. The gain patterns are depicted as two dimensional slices in the zenith and azimuth directions. Additional images of the full three-dimensional gain patterns from which these slices were taken may be seen in

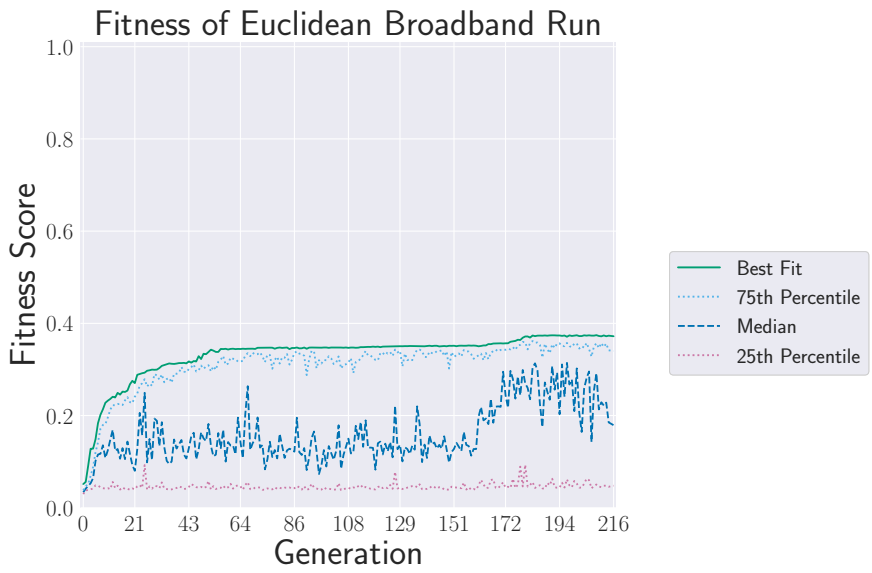

Figure 7. The fitness score of each generation evolving toward a target broadband radiation pattern using the Euclidean distance fitness function. The maximum fitness score and the three quartiles are shown.

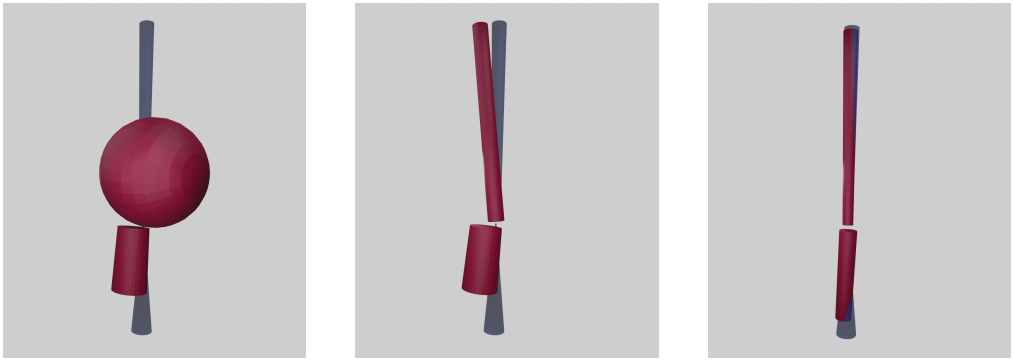

(a) Generation 0 **(b) Generation 5** **(c) Generation 216**

Figure 8. Three example models of the best individuals from generations 0, 5, and 216 are shown, illustrating the evolution of broadband antenna using the Euclidean distance fitness function. The antenna that produced the target gain pattern is given in blue, and the individual is shown in red.

Figures 20-22 in Appendix II.

Figure 10 depicts the phase, in the zenith and azimuth directions, of the most and least fit evolved antennas at the beginning and end of the evolution. Results are again shown for the example frequencies of 200 MHz, 516.73 MHz, and 800.01 MHz. The phase of the most and least fit individuals is represented by the green and blue lines, respectively, while the phase of the target is shown in pink. Additional gain and phase results of the most and least fit individuals at an intermediate generation are displayed in Figures 29 and 30 in Appendix III.

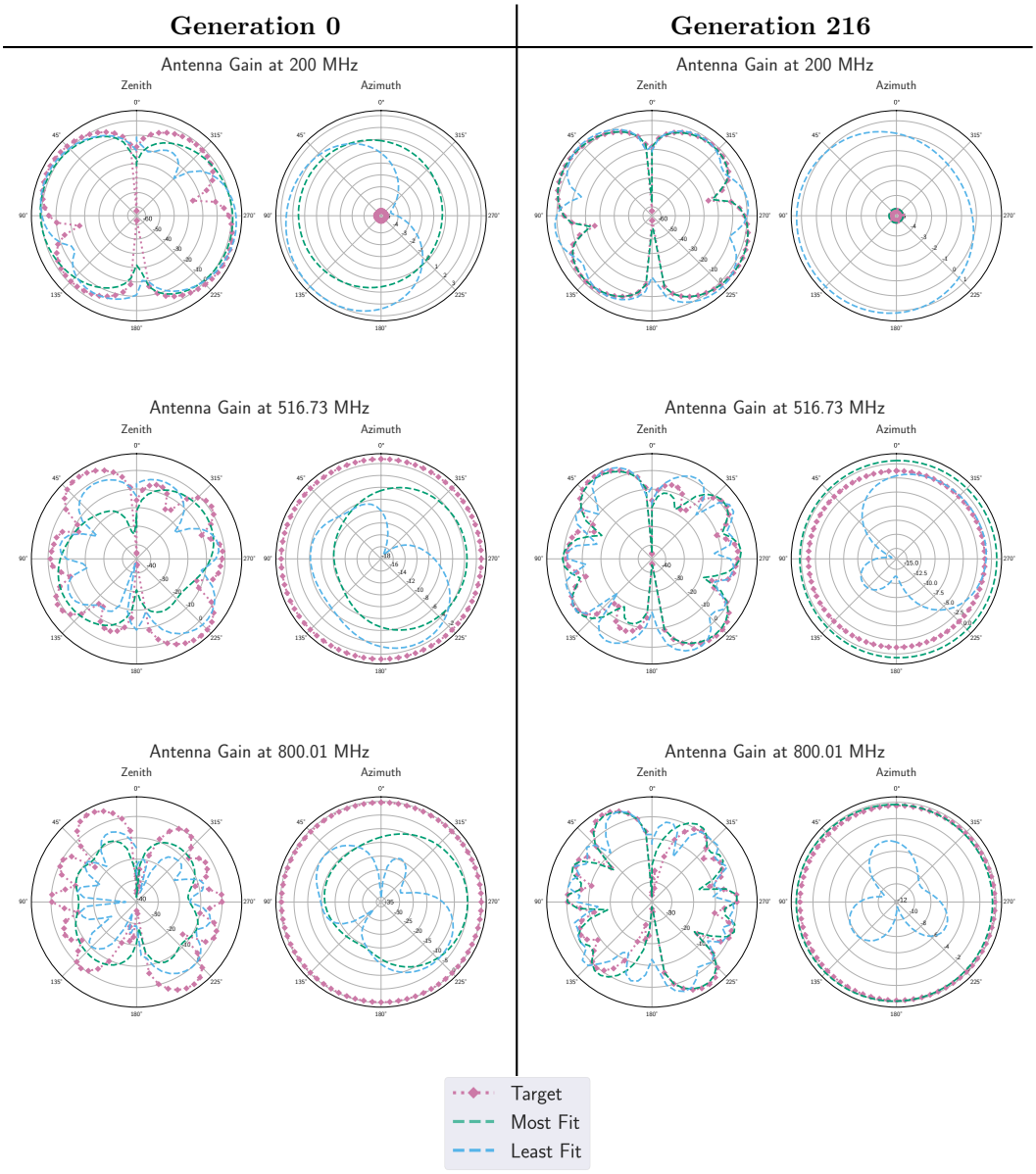

Figure 9. The gain patterns of the most and least fit individuals in generation 0 (left column) and 216 (right column) of the evolution towards a target broadband radiation pattern using the Euclidean distance-based fitness function at three example in-band frequencies: 200 MHz (first row), 516.73 MHz (second row), and 800.01 MHz (third row). The gain pattern of the target is overlaid at the given frequency. Note the target and most fit lines of the Azimuth chart at 200 MHz for generation 216 are overlapping at the center, since the large gain of the least fit indiviudal is increasing the scale of the plot.

The run quickly discovered that individuals constructed with two cylinders approximated the two cones of the design responsible for the target radiation pattern, as evidenced in generation 5 shown in Figure 8. After over 125 generations, the algorithm had yet to change the cylinders to cones, because the replacement mutation was generating new shapes from scratch, resulting in poor fitness individuals. At this

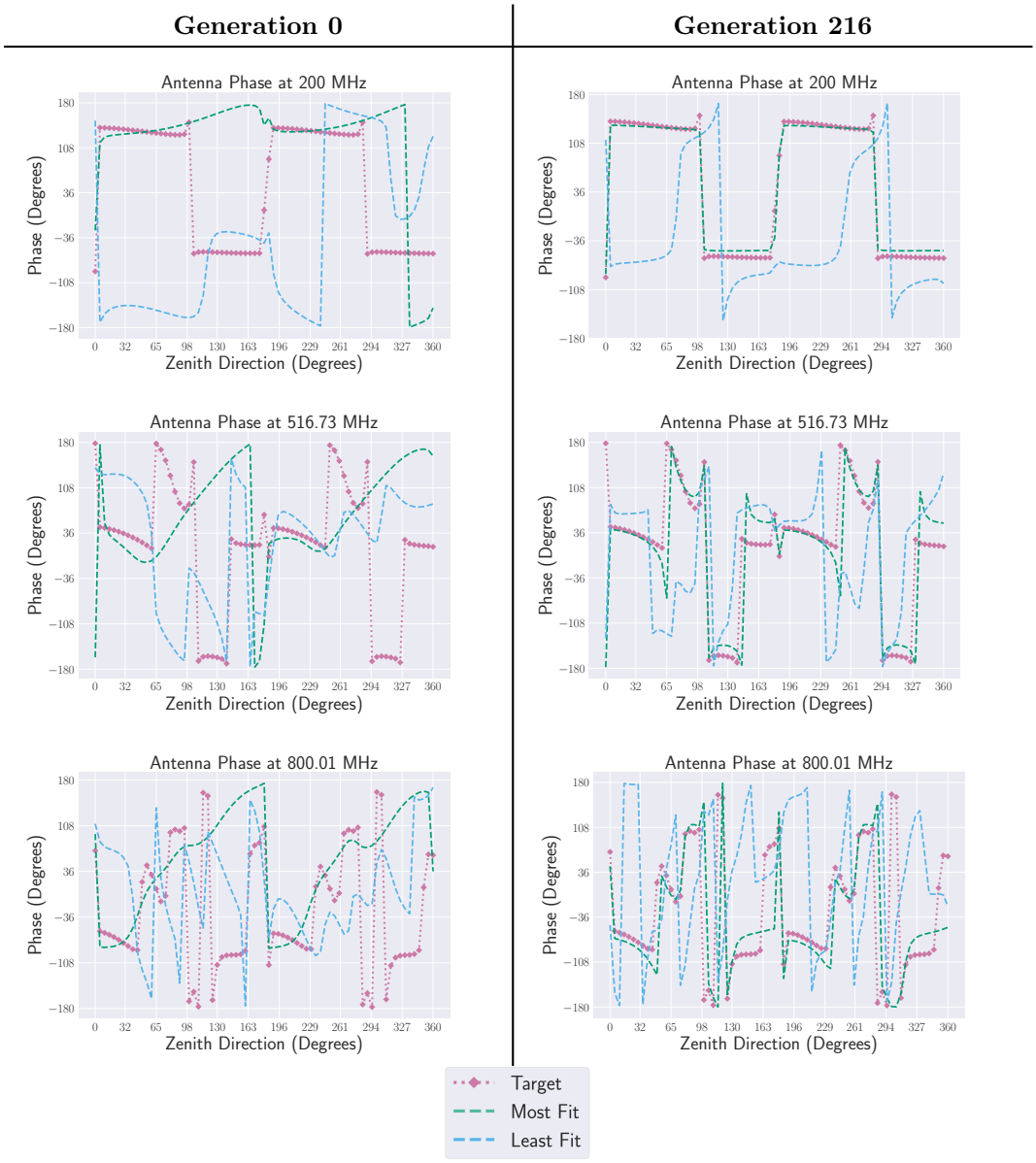

Figure 10. The antenna phase in the zenith direction of the most and least fit individual in generation 0 (left column) and 216 (right column) of the evolution towards a target broadband radiation pattern using the Euclidean distance-based fitness function at three example in-band frequencies: 200 MHz (first row), 516.73 MHz (second row), and 800.01 MHz (third row). Also overlaid on each is the phase of the target at the given frequency.

point, the proportional replacement mutation operator was added in the middle of the run, which facilitated the increase in fitness around generation 175 to a design with two cones. Maximizing the efficiency of the algorithm to avoid plateauing fitness scores in local maxima continues to be a point of emphasis for future development.

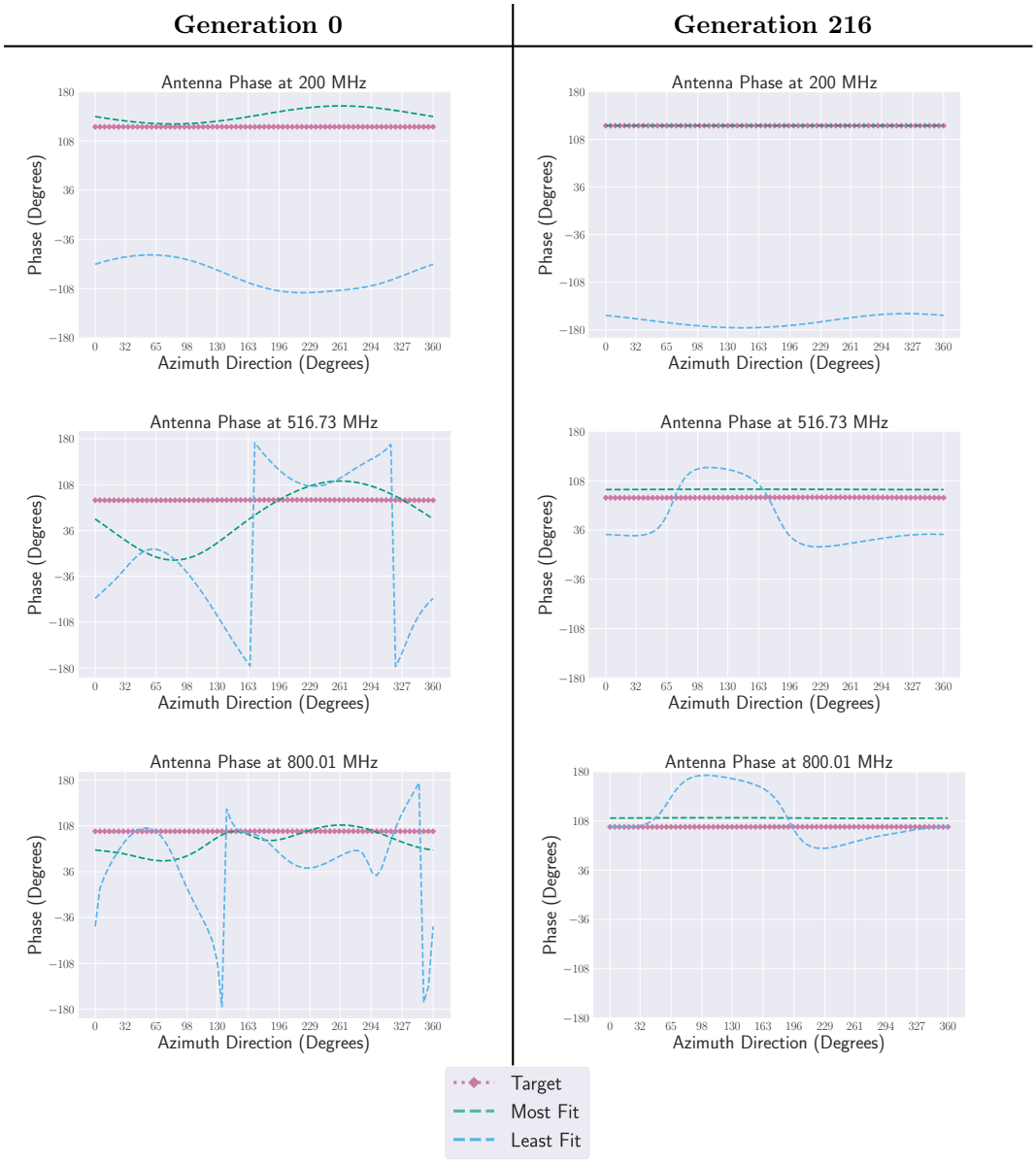

Figure 11. The antenna phase in the azimuth direction of the most and least fit individual in generation 0 (left column) and 216 (right column) of the evolution towards a target broadband radiation pattern using the Euclidean distance-based fitness function at three example in-band frequencies: 200 MHz (first row), 516.73 MHz (second row), and 800.01 MHz (third row). Also overlaid on each is the phase of the target at the given frequency.

B. Directional Gain Fitness Function Results

The next evolution used the directional gain fitness function, which attempted to maximize and/or minimize gain in the specified angular ranges. For this run, the angular ranges for gain maximization and minimization were defined to approximately match the expected sensitivity of a typical dipole antenna. The algorithm targeted maximizing gain between zenith angles of 45° to 135° and minimizing between zenith angles of 0° to 45° and 135° to 180°. The gain in the azimuthal direction did not factor into the fitness score for the purpose of this test. Note that phase did not factor into the directional gain fitness function but could be added based on project or experimental requirements.

1. Single Frequency

Figure 12 shows the results of the directional gain evolution at a single frequency of 300 Mhz. The most fit individual after 142 generations from this evolution achieved a fitness score of approximately 0.87. Figure 13 shows the most fit individuals as of generations 0, 5, 95, and 142, demonstrating how the most fit solution changed throughout the evolution. The individual shown from generation 142 is only slightly improved over generation 95, and while both designs are viable options, the design differences highlight the potential of the GA to find unique solutions, even in this simple case. The evolution will continue to run to explore potential improvements.

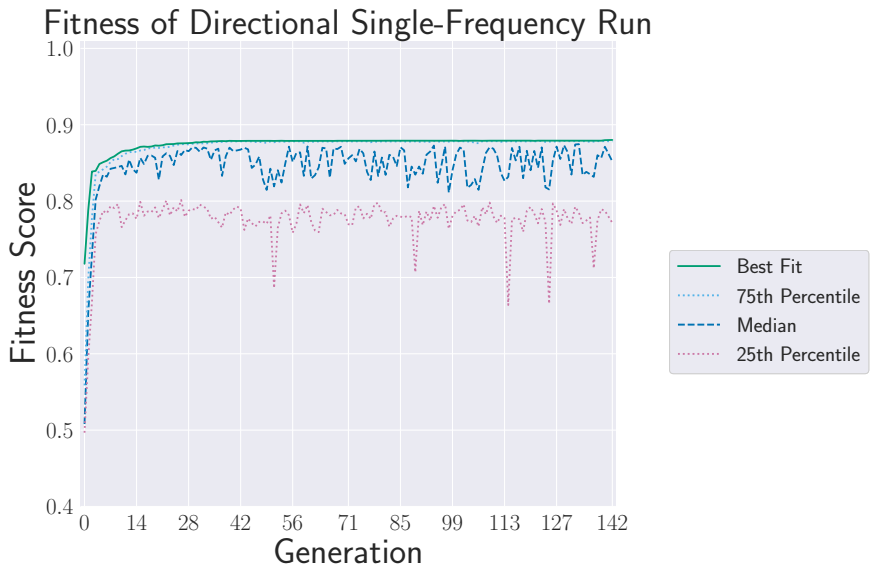

Figure 12. The fitness score of each generation of the single-frequency evolution using the directional gain fitness function. The maximum fitness score and the three quartiles are shown.

Figure 14 depicts the gain patterns of the most and least fit individuals from the population at the beginning and end of the single-frequency directional gain evolution. The most fit individuals are represented by the dashed line and the least fit

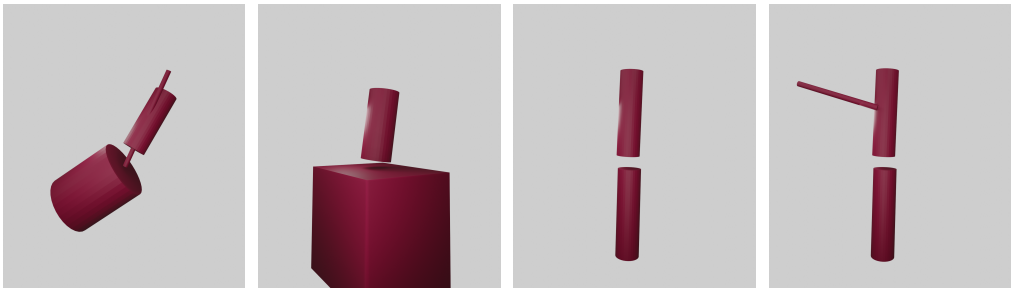

(a) Generation 0 (b) Generation 5 (c) Generation 95 (d) Generation 142

Figure 13. Four example models of the best individual of generations 0, 5, 95, and 142 are shown, illustrating the evolution of the single-frequency antenna using the directional gain fitness function. There is no target antenna since the desired gain pattern was not created from an antenna.

individuals by the dotted line. For reference, the zenith angle ranges specified for gain maximization and minimization are shaded in green and red, respectively. These gain patterns are presented as two-dimensional slices in the zenith and azimuth direction. The corresponding three-dimensional gain patterns for the most fit individual in these generations are available in Figure 23 in Appendix II. An additional set of gain patterns corresponding to the most and least fit individuals in an intermediate generation of the evolution is shown in Figure 31 in Appendix III.

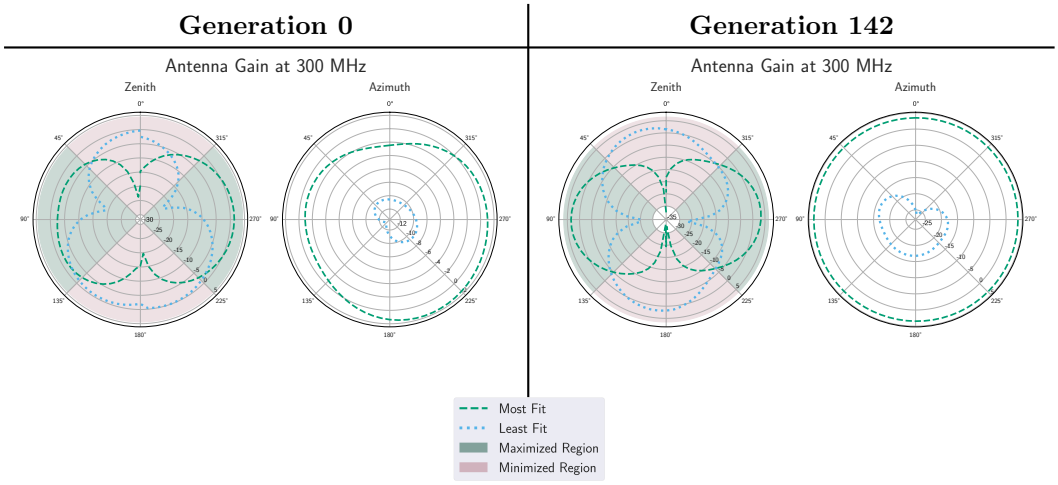

Figure 14. The gain patterns of the most and least fit individual as of generations 0 (left), and 142 (right), of the single-frequency evolution using the directional gain maximization/minimization fitness function. The regions shaded in green and red represent the angular ranges designated for maximization and minimization, respectively.

The single-frequency directional gain evolution achieved a maximum fitness score of approximately 0.88 over 142 generations. The GA quickly ascertained that a dipole-like design performed well in the single-frequency directional gain test, which is expected given that the angular ranges for gain to be maximized were chosen to mimic the gain pattern of a typical dipole antenna. However, in the later generations, the GA discovered an alternative solution that achieved a slightly higher fitness function

(0.8791 versus 0.8801)by adding a third primitive cylinder to the side of the dipole design, as seen in Figure 13. Figure 15 shows the difference in gain patterns between these two designs. The zenith plot patterns appear to show the response patterns closely overlapping, with the additional primitive causing slightly larger gain in the minimization region around 15°, which would reduce the fitness score. The azimuthal plot, which is the horizontal slice of the zenith plot and exists entirely in the maximization region, shows a slight decrease in gain around 90° and larger increase in the maximization region around 270°. The additional primitive caused a slight decrease in some areas but a larger increase in others, resulting in a slightly improved fitness score. This illustrates that despite symmetrical target regions, the algorithm is not restricted to symmetrical designs. This addition to the typical dipole design serves as an example of the GA's potential to discover effective designs that are outside of those that would traditionally be used, and with additional generations new primitives could continue to be added to improve the fitness.

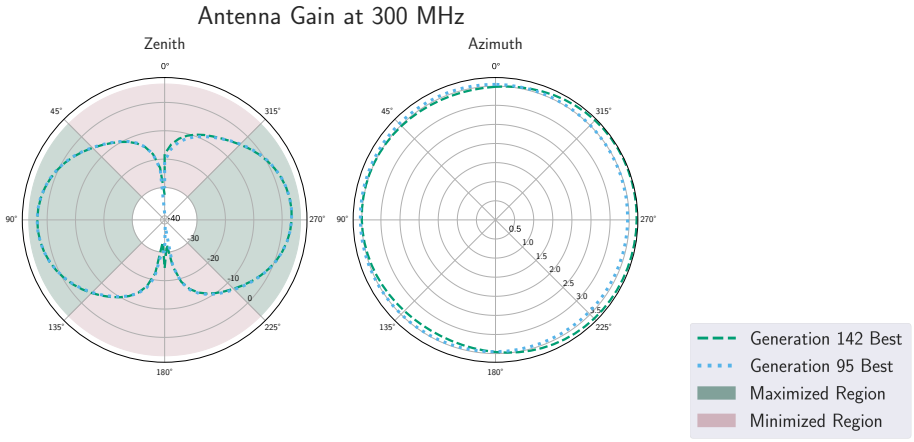

Figure 15. The gain patterns of the most fit individual in generation 95 and generation 142 at 300 MHz using the directional fitness function. The regions shaded in green and red represent the angular ranges designated for maximization and minimization, respectively.

2. Broadband Directional Gain Evolution

Figure 16 shows the results of the broadband directional evolution using the same frequency range of 200 MHz to 800 MHz as the broadband Euclidean distance test. The most fit individual after 229 generations from this evolution achieved a fitness score of approximately 0.82. Figure 17 shows the most fit individuals as of generations 0, 5, and 229, demonstrating how the most fit solution changed throughout the evolution.

Figure 18 depicts the gain patterns of the most and least fit individuals from the population at the beginning and end of the evolution. The most fit individuals are represented by the dashed line and the least fit individuals by the dotted line. For reference, the zenith angle ranges specified for gain maximization and minimization

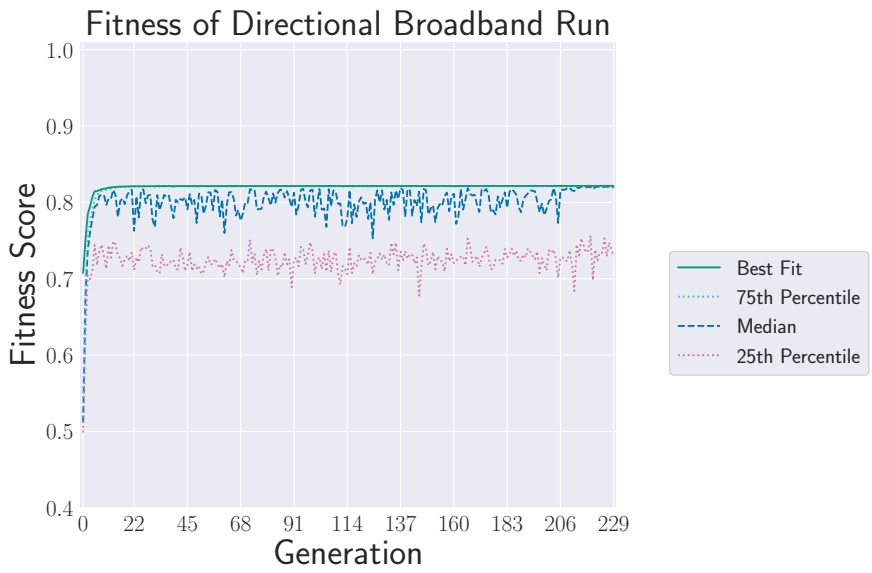

Figure 16. The fitness score of each generation of the broadband evolution using the directional gain fitness function. The maximum fitness score and the three quartiles are shown.

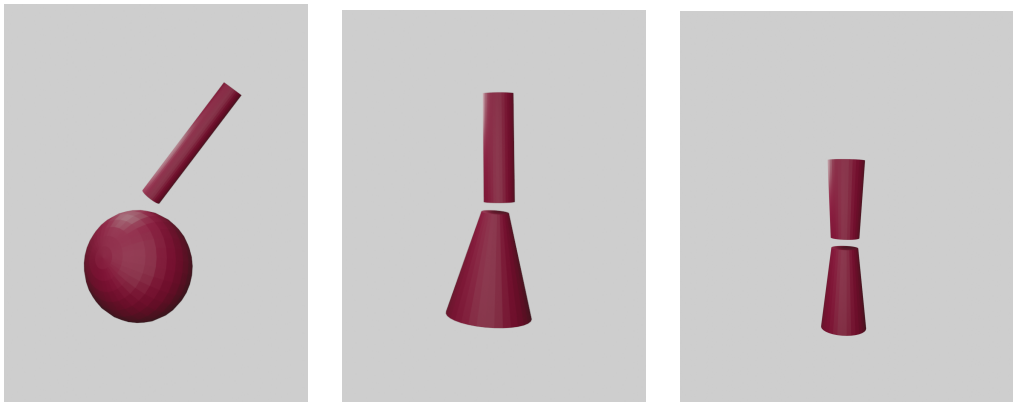

(a) Generation 0 **(b) Generation 5** **(c) Generation 229**

Figure 17. Three example models of the best individual of generations 0, 5, and 229 are shown, illustrating the evolution of broadband antenna using the directional gain fitness function. There is no target antenna since the desired gain pattern was not created from an antenna.

are shaded in green and red, respectively. These gain patterns are presented as two-dimensional slices in the zenith and azimuth direction. The corresponding three-dimensional gain patterns for the most fit individual in these generations are available in Figures 24–26 in Appendix II. An additional set of gain patterns corresponding to the most and least fit individuals in an intermediate generation of the evolution is shown in Figure 32 in Appendix III.

The broadband directional gain evolution achieved a maximum fitness score of approximately 0.82 in 229 generations. The GA quickly arrived at a design of an

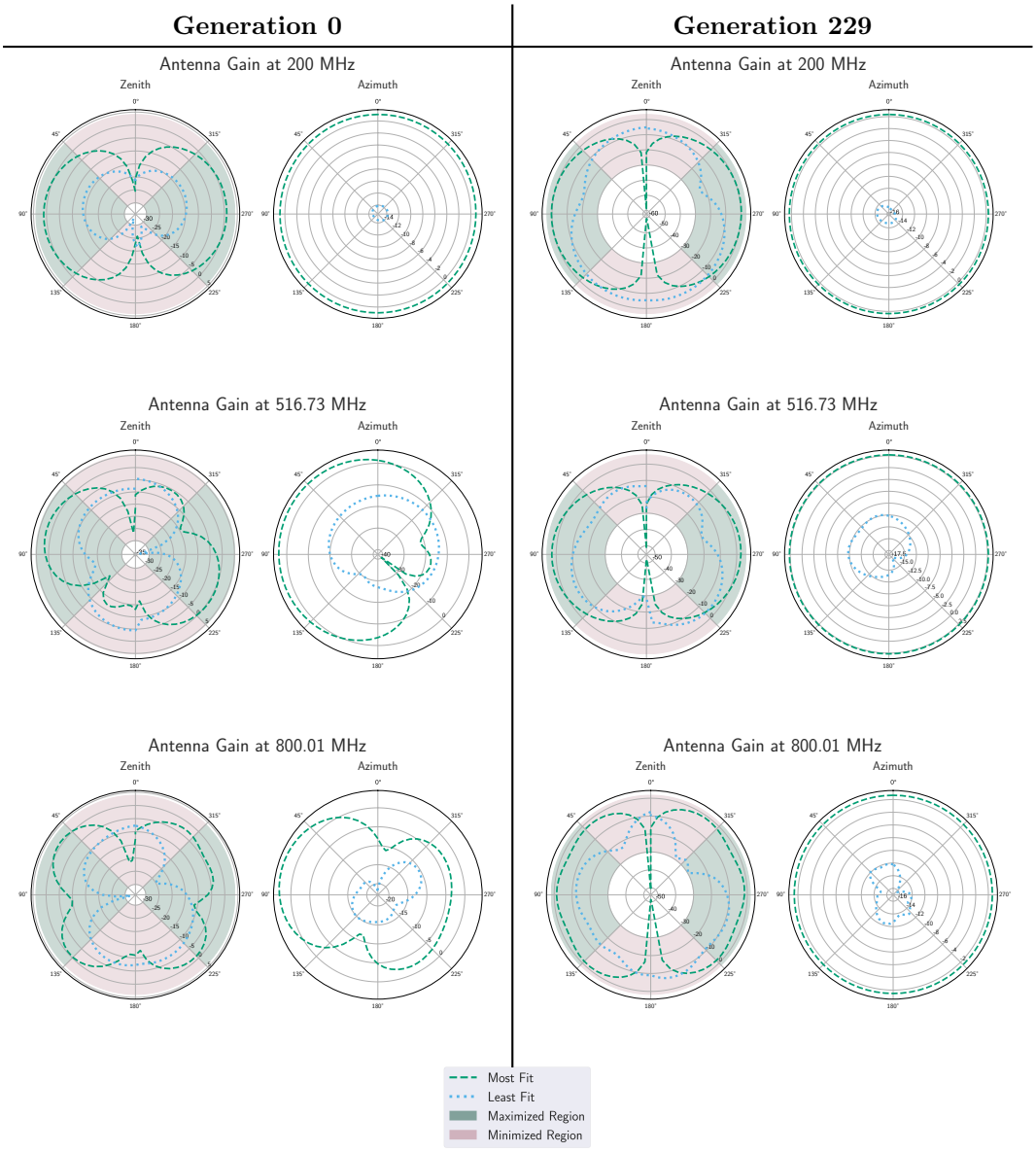

Figure 18. The gain patterns of the most and least fit individuals in generation 0 (left column) and 229 (right column) of the evolution using the directional gain maximization/minimization fitness function at three example in-band frequencies: 200 MHz (first row), 516.73 MHz (second row), and 800.01 MHz (third row). Also overlaid on each is the gain pattern of the target at the given frequency. The regions shaded in green and red represent the angular ranges designated for maximization and minimization, respectively.

individual consisting of a cone and a cylinder in a dipole-like configuration, as depicted in Figure 17, which achieved a fitness score above approximately 0.8. The design was then fine-tuned over many generations, and incremental gains in fitness score were achieved. Given additional generations, an improved solution may likely be found either by additional fine-tuning of the most fit individual's current design or by exploring new or additional primitives.

V. Conclusions

This report presents a GA that can evolve antennas toward desired gain patterns using combinations of smaller component shapes. Tests showed that the algorithm was successful at producing antenna designs based on both the closeness in antenna response to a target antenna gain pattern and an input-desired directional sensitivity. Using a Euclidean distance fitness function, the algorithm was able to evolve antennas to match the gain patterns of dipole antenna. Using a directional gain fitness function the algorithm was able to design antennas to maximize gain between 45° to 135° and minimize between 0° to 45° and 135° to 180°.

A. Future Work

The ultimate goal of this research is to connect antenna design to science outcomes by using fitness functions integrated with science simulation software. Improving the effectiveness of the GA in designing complex and unique antennas for specific functions will also be an area of active development, including allowing other primitive geometries and adding disconnected shapes to act as reflectors and directors. Individuals will also have increased complexity by removing the constraint that allows only one shape per side, by adding additional primitives, and by adding material optimizations including dielectric or metamaterial antennas, such as those discussed in References [55, 56, 57, 58, 59]. Improvements to the GA, such as the addition of the proportional replacement mutation, are in development to improve the speed of convergence and reduce plateaus. The ability to optimize arrays or to produce arrays to achieve improved solutions will be added to the GA. Many experiments have unique or complex design constraints, such as geometry or weight requirements, that will be incorporated into the algorithm in the future.

As the complexity of the algorithm increases it will be critical to continue to optimize the speed of the algorithm and efficiency in converging on final solutions. Appendix V discusses completed and in development improvements to the algorithm by exploring the speed to reach a solution using the shape evolution previously developed as a test case. This testing was used to validate the steady-state, elite, and forced diversity changes to the algorithm. In development is the use of adaptable dynamic genetic operators, where reinforced learning is used to change how individuals are created based on the current environment of the run.

More advanced improvements to the algorithm will also be investigated, including particle swarms and other heuristic methods [60, 61, 62, 63], or neural networks [64, 65], to improve efficiency. Particle swarms could help reduce the number of ineffective individuals being generated and help to converge on a solution more quickly. A neural network could be used to predict the fitness of individuals similar to previously tested individuals and reduce the computational time needed to simulate performance and calculate fitness.

The work presented in this report demonstrates a genetic algorithm that can evolve antennas with desired gain patterns from primitive shapes. Continued research in this area will allow for optimization of designs for science outcomes with reduced cost and scheduling.

Acknowledgments

The research was carried out at the Jet Propulsion Laboratory, California Institute of Technology, under a contract with the National Aeronautics and Space Administration (80NM0018D0004). The authors are grateful to the entire GENETIS collaboration for their prior work and continued assistance, especially Prof. Wolfgang Banzhaf. We would also like to thank Remcom for their support, especially Tarun Chawla, Walter Janusz, and Benjamin Hardy.

References

[1] J. Rolla, B. Reynolds, J. Weiler, A. Connolly, R. Debolt, A. Machtay, B. Sipe, and D. Wells, "Design of 3D Antenna Geometries Using Genetic Algorithms," *The Interplanetary Network Progress Report*, vol. 42-234, pp. 1–26, August 2023.

[2] R. Luebbers, "XFDTD and beyond-from classroom to corporation," *2006 IEEE Antennas and Propagation Society International Symposium*, pp. 119–122, 2006.

[3] F. Tamjid, F. Foroughian, C. M. Thomas, A. Ghahreamani, R. Kazemi, and A. E. Fathy, "Toward high-performance wideband gnss antennas-design tradeoffs and development of wideband feed network structure," *IEEE Transactions on Antennas and Propagation*, vol. 68, no. 8, pp. 5796–5806, 2020.

[4] B. R. Rao, *GPS/GNSS Antennas*. Artech House, 2013.

[5] J. J. H. Wang, "Antennas for global navigation satellite system (gnss)," *Proceedings of the IEEE*, vol. 100, no. 7, pp. 2349–2355, 2012.

[6] A. Romero-Wolf, S. Vance, F. Maiwald, E. Heggy, P. Ries, and K. Liewer, "A passive probe for subsurface oceans and liquid water in jupiter's icy moons," *Icarus*, vol. 248, pp. 463–477, 2015. https://www.sciencedirect.com/science/article/pii/S0019103514006009

[7] D. M. Schroeder, A. Romero-Wolf, L. Carrer, C. Grima, B. A. Campbell, W. Kofman, L. Bruzzone, and D. D. Blankenship, "Assessing the potential for passive radio sounding of europa and ganymede with rime and reason," *Planetary and Space Science*, vol. 134, pp. 52–60, 2016. https://www.sciencedirect.com/science/article/pii/S0032063316301465

[8] R. Prechelt, A. Romero-Wolf, P. Gorham, E. Costello, R. Ghent, and P. Lucey, "Radio detection of subsurface lunar ice via the askaryan effect with the cosmic ray lunar sounder (corals)," *AGU Fall Meeting Abstracts*, pp. P41C–09, 2021.

[9] W. M. Farrell, M. D. Desch, and P. Zarka, "On the possibility of coherent cyclotron emission from extrasolar planets," *JGR Planets*, vol. 104(E6), pp. 14 025–14 032, June 1999.

[10] P. Zarka, R. A. Treumann, B. P. Ryabov, and V. B. Ryabov, "Magnetically-driven planetary radio emissions and application to extrasolar planets," *APSS*, vol. 277, pp. 293–300, June 2001.

[11] T. J. W. Lazio and W. M. Farrell, "Radio detection of extrasolar planets: present and future prospects," *Planetary Radio Emissions VI*, pp. 603–610, 2006.

[12] E. Feenberg and H. Primakoff, "Interaction of cosmic-ray primaries with sunlight and starlight," *Physical Review*, vol. 73(5), pp. 449–469, March 1948.

[13] J. E. Felten and P. Morrison, "Omnidirectional inverse compton and synchrotron radiation from cosmic distributions of fast electrons and thermal photons," *Astrophysical Journal*, vol. 146, p. 686, December 1966.

[14] M. J. Rees, "Studies in radio source structure-III. Inverse Compton radiation from radio sources," *mnras*, vol. 137, p. 429, January 1967.

[15] G. R. Blumenthal and R. J. Gould, "Bremsstrahlung, synchrotron radiation, and Compton scattering of high-energy electrons traversing dilute gases," *Reviews of Modern Physics*, vol. 42(2), pp. 237–271, January 1970.

[16] L. Feretti and G. Giovannini, "Diffuse cluster radio sources (review)," *Proceedings of the 175th Symposium of the International Astronomical Union*, vol. 175, p. 333, January 1996.

[17] S. R. Furlanetto, S. P. Oh, and F. H. Briggs, "Cosmology at low frequencies: the 21 cm transition and the high-redshift Universe," *Physics Report*, vol. 433(4-6), pp. 181–301, October 2006.

[18] J. R. Pritchard and A. Loeb, "Evolution of the 21cm signal throughout cosmic history," *Physical Review D*, vol. 78(10), p. 103511, November 2008.

[19] J. R. Pritchard and A. Loeb, "Constraining the unexplored period between the dark ages and reionization with observations of the global 21 cm signal," *Physical Review D*, vol. 82(2), p. 023006, July 2010.

[20] A. Liu, J. R. Pritchard, M. Tegmark, and A. Loeb, "Global 21 cm signal experiments: a designer's guide," *Physical Review D*, vol. 87(4), p. 043002, February 2013.

[21] B. Alhijawi and A. Awajan, "Genetic algorithms: Theory, genetic operators, solutions, and applications," *Evolutionary Intelligence*, pp. 1–12, 2023.

[22] S. K. Goudos, D. E. Anagnostou, C. Kalialakis, P. Vasant, S. Nikolaou *et al.*, "Evolutionary algorithms applied to antennas and propagation: emerging trends and applications," *International Journal of Antennas and Propagation*, vol. 2016, 2016.

[23] B. Liu, H. Hu, H. Han, H. Lv, and L. Li, "Optimization of the design of gas cherenkov detectors for icf diagnosis," *Nuclear Instruments and Methods in Physics Research Section A: Accelerators, Spectrometers, Detectors and Associated Equipment*, vol. 897, pp. 54–58, July 2018.

[24] A. Liu, A. Bross, and D. Neuffer, "Optimization of the magnetic horn for the nuSTORM non-conventional neutrino beam using the genetic algorithm," *Nuclear Inst. and Methods in Physics Research, A*, vol. 794, pp. 200–205, 2015.

[25] G. Oliveri, P. Rocca, L. Poli, M. Carlin, E. T. Bekele, A. De Matteis, and A. Massa, "Evolutionary strategies for advanced array optimization," *2011 IEEE International Symposium on Antennas and Propagation (APSURSI)*, pp. 2441–2444, 2011.

[26] F. Grimaccia, M. Mussetta, A. Niccolai, and R. E. Zich, "Comparison of binary evolutionary algorithms for optimization of thinned array antennas," *2018 IEEE Congress on Evolutionary Computation (CEC)*, pp. 1–8, 2018.

[27] Q. Xu, S. Zeng, F. Zhao, R. Jiao, and C. Li, "On formulating and designing antenna arrays by evolutionary algorithms," *IEEE Transactions on Antennas and Propagation*, vol. 69, no. 2, pp. 1118–1129, 2021.

[28] J. Rolla, A. Machtay, A. Patton, W. Banzhaf, A. Connolly, R. Debolt, L. Deer, E. Fahimi, E. Ferstle, P. Kuzma, C. Pfendner, B. Sipe, K. Staats, and S. A. Wissel, "Using evolutionary algorithms to design antennas with greater sensitivity to ultra high energy neutrinos," *Physical Review D*, 2023, forthcoming.

[29] B. Reynolds, J. Rolla, A. Machtay, W. Banzhaf, D. Calderon, C. Chen, A. Connolly, R. Debolt, E. Fahimi, N. King, E. Melotti, A. Patton, B. Sipe, K. Staats, D. Wells, S. Wissel, and A. Zinn, "Design of antennas with greater sensitivity to ultra-high energy neutrinos," *National Radio Science Meeting*, 1 2023.

[30] A. Machtay, J. Rolla, and A. Patton, "Using genetic algorithms to optimize antenna designs for improved sensitivity to ultra-high energy neutrinos," *38th International Cosmic Ray Conference*, 2023.

[31] J. Rolla, D. Arakaki, M. Clowdus, A. Connolly, R. Debolt, L. Deer, E. Fahimi, E. Ferstl, S. Gourapura, C. Harris, L. Letwin, A. Machtay, A. Patton, C. Pfendner, C. Sbrocco, T. Sinha, B. Sipe, K. Staats, J. Trevithick, and S. Wissel, "Evolving antennas for ultra-high energy neutrino detection," *37th International Cosmic Ray Conference*, 2021.

[32] J. Rolla, A. Connolly, K. Staats, S. Wissel, D. Arakaki, I. Best, A. Blenk, B. Clark, M. Clowdus, S. Gourapura, C. Harris, H. Hasan, L. Letwin, D. Liu, C. Pfendner, J. Potter, C. Sbrocco, T. Sinha, and J. Trevithick, "Evolving antennas for ultra-high energy neutrino detection," *36th International Cosmic Ray Conference*, 2019.

[33] D. McCarthy, N. Trappe, J. A. Murphy, C. O'Sullivan, M. Gradziel, S. Doherty, P. G. Huggard, A. Polegro, and M. van der Vorst, "The optimisation, design and verification of feed horn structures for future cosmic microwave background missions," *Infrared Physics & Technology*, vol. 76, pp. 32–37, 2016.

[34] M. Calviani, S. di Luise, V. Galymov, and P. Velten, "Optimization of neutrino fluxes for future long baseline neutrino oscillation experiments," *Nuclear and Particle Physics Proceedings, 37th International Conference on High Energy Physics*, vol. 273-275, pp. 2681–2683, 2016.

[35] H. Schellman, "LBNF beamline," *39th International Conference on High Energy Physics*, vol. 340, 2018.

[36] A. G. Baydin, K. Cranmer, P. d. C. Manzano, C. Delaere, D. Derkach, J. Donini, T. Dorigo, A. Giammanco, J. Kieseler, L. Layer, G. Louppe, F. Ratnikov, G. C. Strong, M. Tosi, A. Ustyuzhanin, P. Vischia, and H. Yarar, "Toward machine learning optimization of experimental design," *Nuclear Physics News*, vol. 31(1), pp. 25–28, 2021.

[37] D. Kastanya, "ADORE-GA: genetic algorithm variant of the ADORE algorithm for ROP detector layout optimization in CANDU reactors," *Annals of Nuclear Energy*, vol. 46, pp. 160–168, 2012.

[38] E. B. Flynn and M. D. Todd, "Optimal placement of piezoelectric actuators and sensors for detecting damage in plate structures," *Journal of Intelligent Material Systems and Structures*, vol. 21(3), pp. 265–274, 2010.

[39] N. Kleedtke, M. Hua, and S. Pozzi, "Genetic algorithm optimization of tin–copper graded shielding for improved plutonium safeguards measurements." *Nuclear Inst. and Methods in Physics Research, A*, vol. 988, 2021.

[40] S. Abdullin, "Genetic algorithm for SUSY trigger optimization in CMS detector at LHC," *Nuclear Instruments and Methods in Physics Research Section A: Accelerators, Spectrometers, Detectors and Associated Equipment*, vol. 502(2), pp. 693–695, 2003, Proceedings of the VIII International Workshop on Advanced Computing and Analysis Techniques in Physics Research.

[41] J. Frenzel, "Genetic algorithms," *IEEE Potentials*, vol. 12(3), pp. 21–24, 1993.

[42] K. Man, K. Tang, and S. Kwong, "Genetic algorithms: concepts and applications [in engineering design]," *IEEE Transactions on Industrial Electronics*, vol. 43(5), pp. 519–534, 1996.

[43] D. Beasley, D. R. Bull, and R. R. Martin, "An overview of genetic algorithms: Part 1, fundamentals," *University computing*, vol. 15, no. 2, pp. 56–69, 1993.

[44] B. O. Community, *Blender - a 3D modelling and rendering package*, Blender Foundation, Stichting Blender Foundation, Amsterdam, 2018. http://www.blender.org

[45] J. Pan, S. Chitta, and D. Manocha, "Fcl: A general purpose library for collision and proximity queries," *2012 IEEE International Conference on Robotics and Automation*, pp. 3859–3866, 2012, accessed at: https://github.com/flexible-collision-library.

[46] "Remcom, personal communication," 2022.

[47] *IEEE Standard for Definitions of Terms for Antennas*, 2014.

[48] J. Zhong, X. Hu, J. Zhang, and M. Gu, "Comparison of performance between different selection strategies on simple genetic algorithms," *International Conference on Computational Intelligence for Modelling, Control and Automation and International Conference on Intelligent Agents, Web Technologies and Internet Commerce (CIMCA-IAWTIC'06)*, vol. 2, pp. 1115–1121, 2005.

[49] A. Shuckla, H. M. Pandey, and D. Mehrotra, "Comparative review of selection techniques in genetic algorithm." *2015 International Conference on Futuristic Trends on Computational Analysis and Knowledge Management (ABLAZE)*, pp. 515–519. IEEE, 2015.

[50] B. L. Miller, D. E. Goldberg *et al.*, "Genetic algorithms, tournament selection, and the effects of noise," *Complex systems*, vol. 9, no. 3, pp. 193–212, 1995.

[51] D. E. Goldberg and K. Deb, *A Comparative Analysis of Selection Schemes Used in Genetic Algorithms*, ser. Foundations of Genetic Algorithms, G. J. Rawlins, Ed. Elsevier, 1991, vol. 1. https://www.sciencedirect.com/science/article/pii/B9780080506845500082

[52] E. O. Scott and K. A. De Jong, "Understanding simple asynchronous evolutionary algorithms," *Proceedings of the 2015 ACM Conference on Foundations of Genetic Algorithms XIII*, p. 85–98, 2015. https://doi.org/10.1145/2725494.2725509

[53] E. Scott, M. Coletti, C. Schuman, B. Kay, S. Kulkarni, M. Parsa, and K. De Jong, "Avoiding excess computation in asynchronous evolutionary algorithms," *20th UK Workshop on Computational Intelligence*, vol. 1409, 11 2021. https://www.osti.gov/biblio/1845800

[54] E. Scott and K. De Jong, "Initialization matters for asynchronous steady-state evolutionary algorithms," *Proceedings of the Companion Conference on Genetic and Evolutionary Computation*, p. 1570–1578, 2023. https://doi.org/10.1145/3583133.3596404

[55] S. M. Hanham, T. S. Bird, A. D. Hellicar, and R. A. Minasian, "Evolved-profile dielectric rod antennas," *IEEE Transactions on Antennas and Propagation*, vol. 59(4), pp. 1113–1122, 2011.

[56] M. A. Belen and P. Mahouti, "Design of nonuniform substrate dielectric lens antennas using 3d printing technology," *Microwave and Optical Technology Letters*, vol. 62(2), pp. 756–762, 2020. https://onlinelibrary.wiley.com/doi/abs/10.1002/mop.32065

[57] M. Tam and R. D. Murch, "Half volume dielectric resonator antenna designs," *Electronics Letters*, vol. 33(23), pp. 1914–1916, 1997.

[58] R. W. Ziolkowski, P. Jin, and C.-C. Lin, "Metamaterial-inspired engineering of antennas," *Proceedings of the IEEE*, vol. 99(10), pp. 1720–1731, 2010.

[59] A. Erentok and R. W. Ziolkowski, "Metamaterial-inspired efficient electrically small antennas," *IEEE Transactions on Antennas and Propagation*, vol. 56(3), pp. 691–707, 2008.

[60] Y. Zhang, S. Wang, and G. Ji, "A comprehensive survey on particle swarm optimization algorithm and its applications," *Mathematical Problems in Engineering*, vol. 2015, p. 931256, Oct 2015. https://doi.org/10.1155/2015/931256.

[61] D. Wang, D. Tan, and L. Liu, "Particle swarm optimization algorithm: an overview," *Soft computing*, vol. 22, pp. 387–408, 2018.

[62] G. Papazoglou and P. Biskas, "Review and comparison of genetic algorithm and particle swarm optimization in the optimal power flow problem," *Energies*, vol. 16(3), p. 1152, 2023.

[63] R. Thangaraj, M. Pant, A. Abraham, and P. Bouvry, "Particle swarm optimization: hybridization perspectives and experimental illustrations," *Applied Mathematics and Computation*, vol. 217(12), pp. 5208–5226, 2011.

[64] Y. Jin, "A comprehensive survey of fitness approximation in evolutionary computation," *Soft computing*, vol. 9(1), pp. 3–12, 2005.

[65] F. van den Bergh and A. Engelbrecht, "A cooperative approach to particle swarm optimization," *IEEE Transactions on Evolutionary Computation*, vol. 8(3), pp. 225–239, 2004.

[66] J. Quevedo, M. Abdelatti, F. Imani, and M. Sodhi, "Using reinforcement learning for tuning genetic algorithms," *Proceedings of the Genetic and Evolutionary Computation Conference*, New York, NY, USA, p. 1503–1507, 2021. https://doi.org/10.1145/3449726.3463203

APPENDICES

I. Individual Genes and Genetic Algorithm Parameters

Table 1. Parameters used in Genetic Algorithm

Category	Type	Parameters
General	Run	Num. Individuals, Num. Generations, Fitness Function, Target pattern, Steady-state flag, Forced diversity flag
	Individual	Max. Tree Depth, Max. Shapes, Shell thickness
	XFdtd	Frequency range, Frequency step
Shape	Cuboid	Shape allowed, Length, Width, and Height Ranges
	Sphere	Shape allowed, Radius Range
	Cylinder	Shape allowed, Radius, and Height Range
	Cone	Shape allowed, Radius 1, Radius 2, and Height Range
Selection Methods	Tournament	Percent of parents, Group Size
	Roulette	Percent of parents
	Rank	Percent of parents
Genetic Operators	Dim. Mutation	Percent of children, St. Dev. %
	Rotation Mutation	Percent of children, St. Dev. %
	Location Mutation	Percent of children, St. Dev. %
	Grow Mutation	Percent of children
	Prune Mutation	Percent of children
	Regen. Mutation	Percent of children
	Side Switch	Percent of children
	Gene Crossover	Percent of children
	Branch Crossover	Percent of children
	Reproduction	Percent of children
	Injection	Percent of children

Table 2. Primitive shape genes

Gene	**Values**
Shape Type	Cuboid, Cylinder, Cone, Sphere
Dimensions	Varies by shape type (See Table 3)
Location	Cartesian coordinates of shape midpoint
Rotation	θ, ϕ
Connected From	Shape built from
Connected To	Side that shapes are attached to

Table 3. Dimensions for each shape type

Shape Type	**Dimension Genes**
Cuboid	Length, Width, Height
Cylinder	Radius, Height
Cone	Inner Radius, Outer Radius, Height
Sphere	Radius

II. 3-Dimensional Gain Patterns

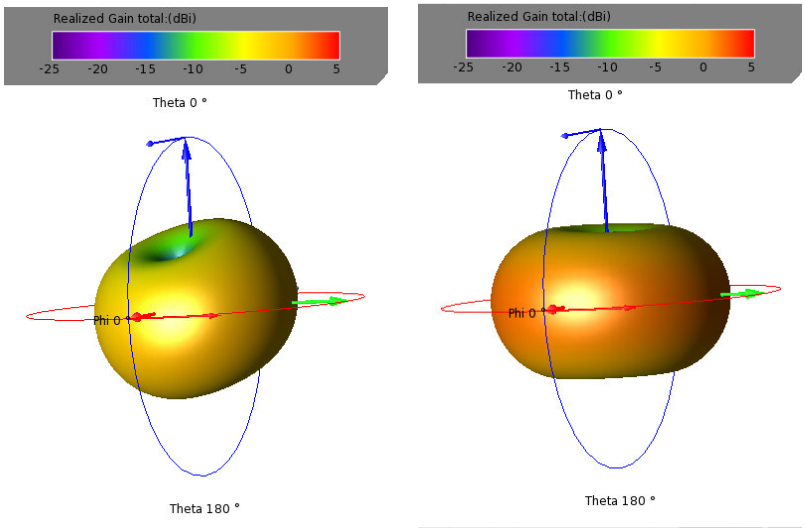

(a) Generation 0

(b) Generation 25

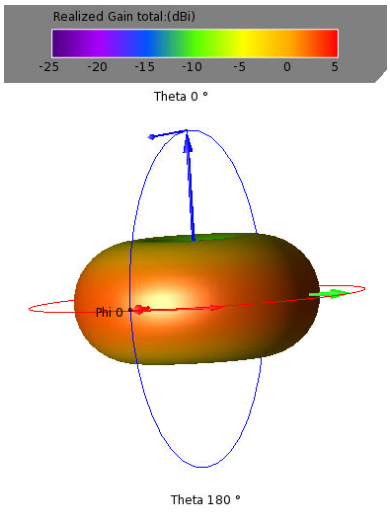

(c) Generation 441

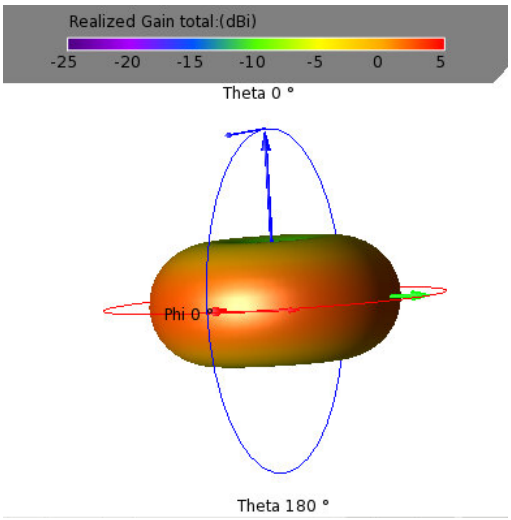

(d) Target

Figure 19. The antenna gain pattern of the most fit individual as of generations 0 (a), 25 (b), and 441 (c) of the single-frequency evolution towards a target radiation pattern (d) using the Euclidean distance-based fitness function.

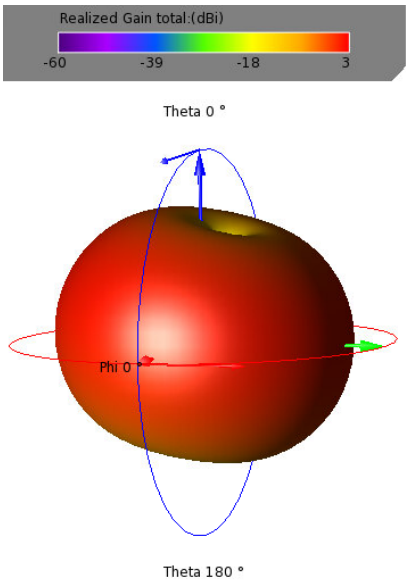

(a) Generation 0
200 MHz

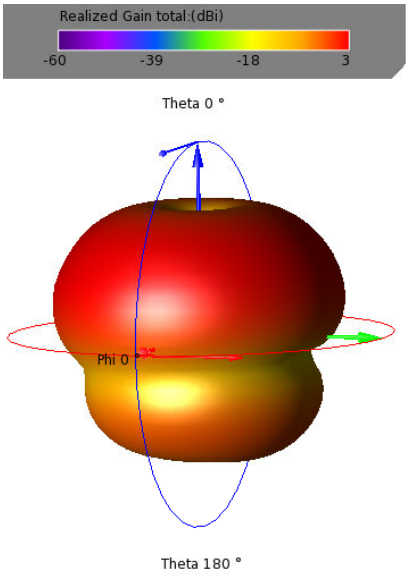

(b) Generation 5
200 MHz

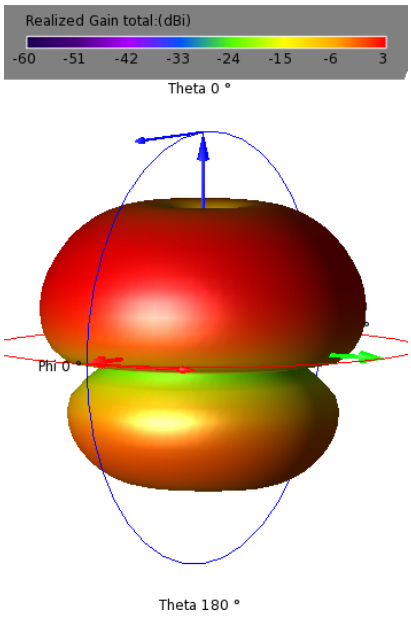

(c) Generation 216
200 MHz

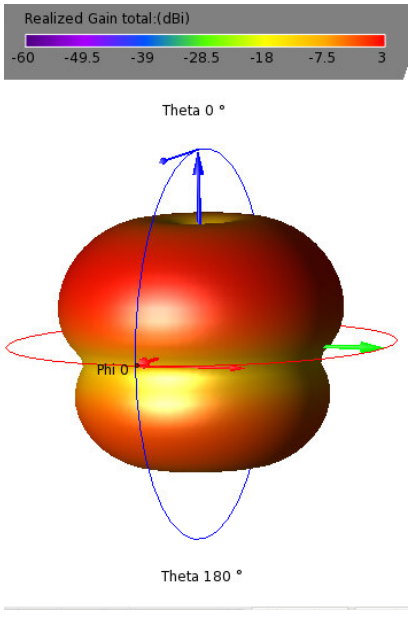

(d) Target
200 MHz

Figure 20. The antenna gain pattern of the most fit individual as of generations 0 (a), 5 (b), and 216 (c) of the broadband evolution towards a target radiation pattern (d) using the Euclidean distance-based fitness function. Shown here are the gain patterns corresponding to a frequency of 200 MHz.

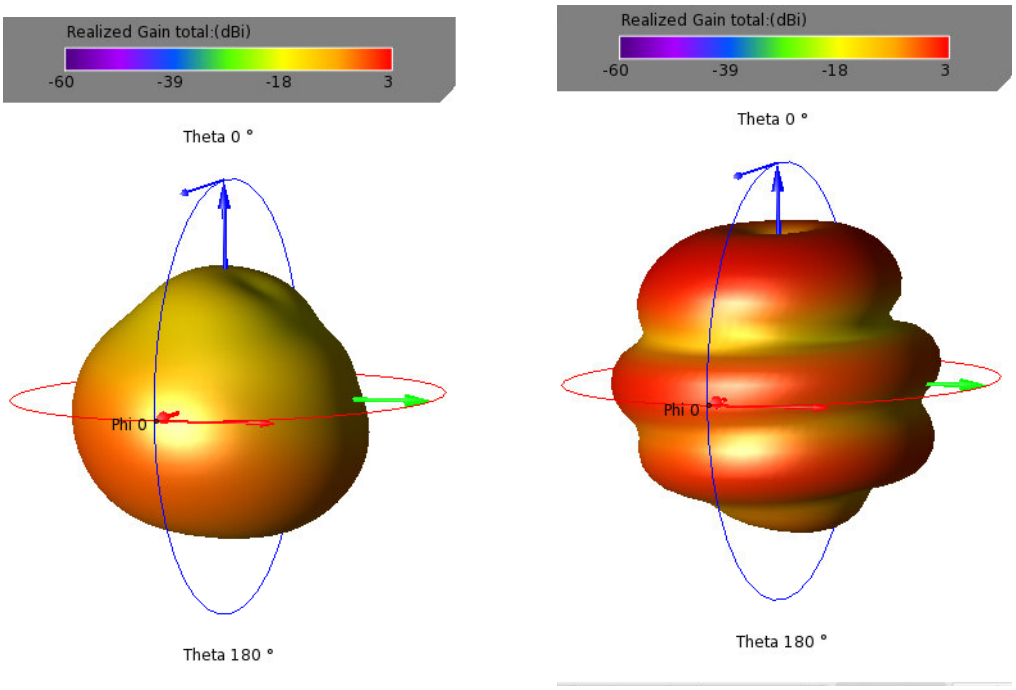

(a) Generation 0
516.73 MHz

(b) Generation 5
516.73 MHz

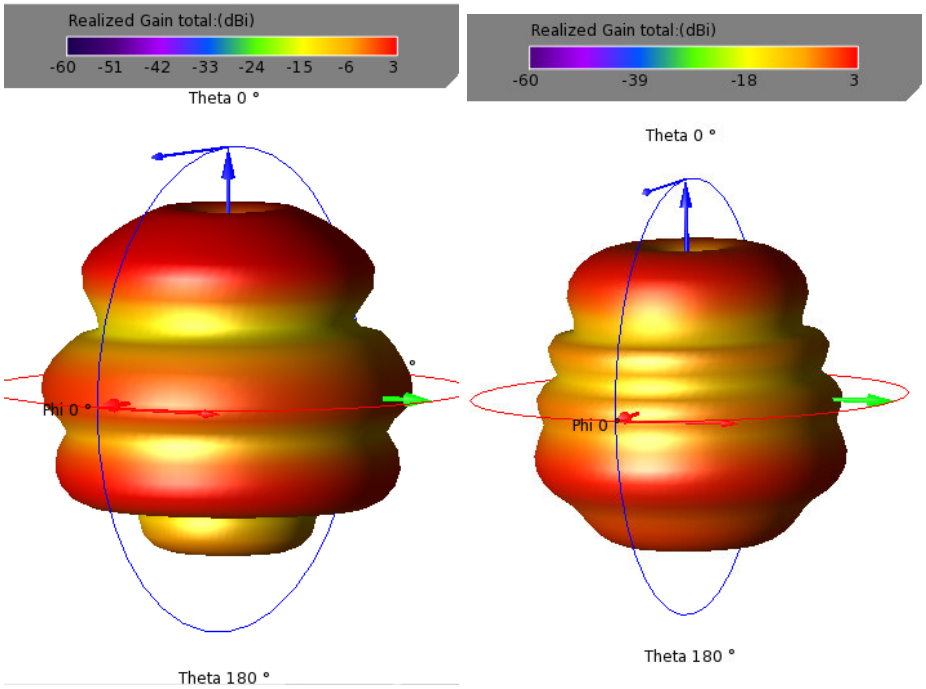

(c) Generation 216
516.73 MHz

(d) Target
516.73 MHz

Figure 21. The antenna gain pattern of the most fit individual as of generations 0 (a), 5 (b), and 216 (c) of the broadband evolution towards a target radiation pattern (d) using the Euclidean distance-based fitness function. Shown here are the gain patterns corresponding to a frequency of 516.73 MHz.

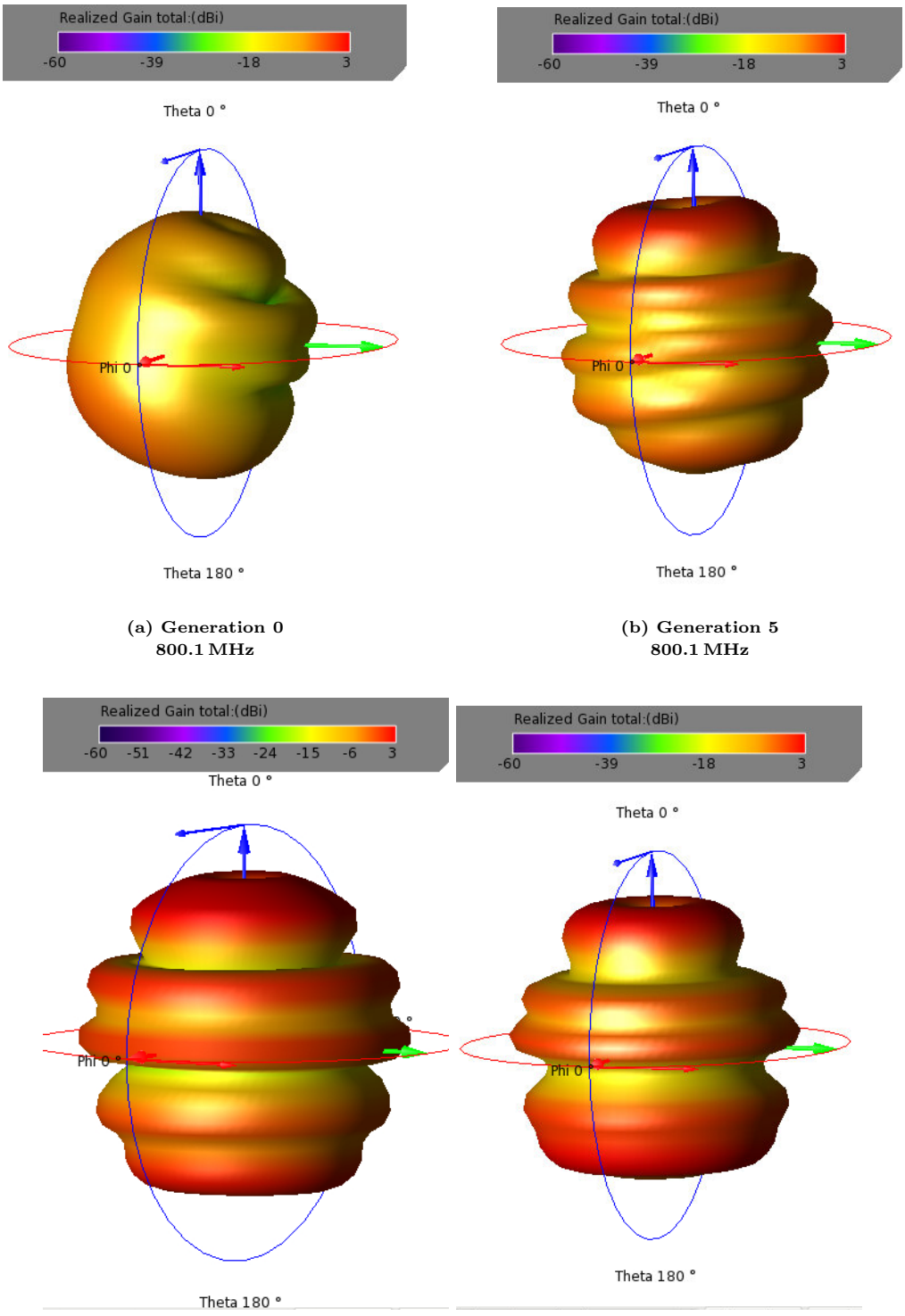

(a) Generation 0
800.1 MHz

(b) Generation 5
800.1 MHz

(c) Generation 216
800.1 MHz

(d) Target
800.1 MHz

Figure 22. The antenna gain pattern of the most fit individual as of generations 0 (a), 5 (b), and 216 (c) of the broadband evolution towards a target radiation pattern (d) using the Euclidean distance-based fitness function. Shown here are the gain patterns corresponding to a frequency of 800.1 MHz.

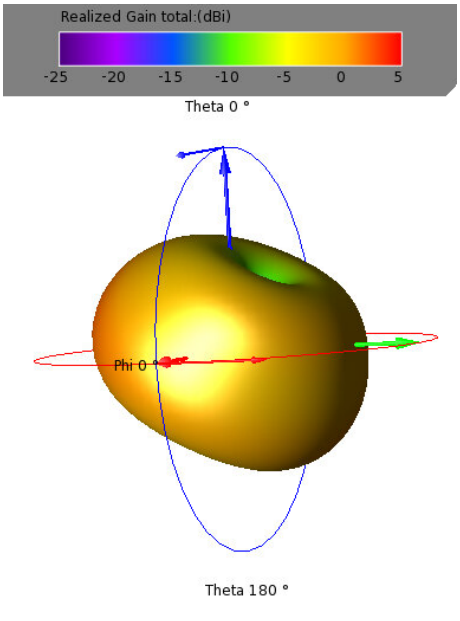

(a) Generation 0

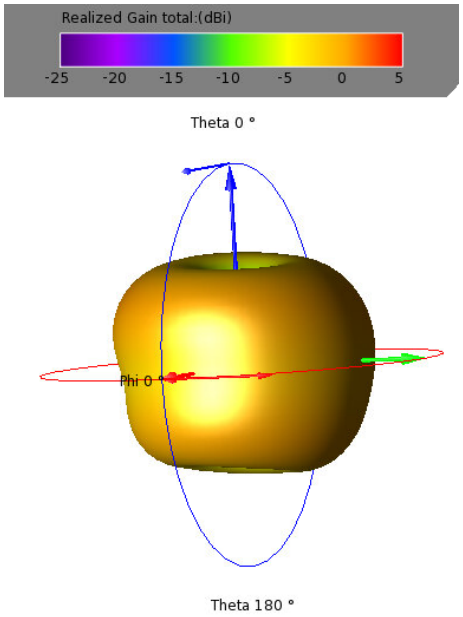

(b) Generation 5

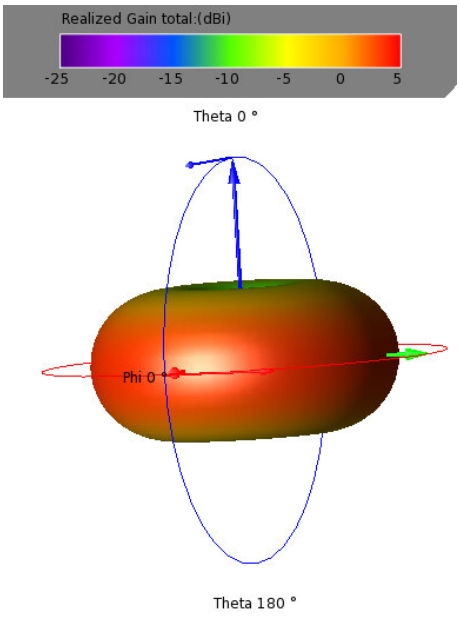

(c) Generation 95

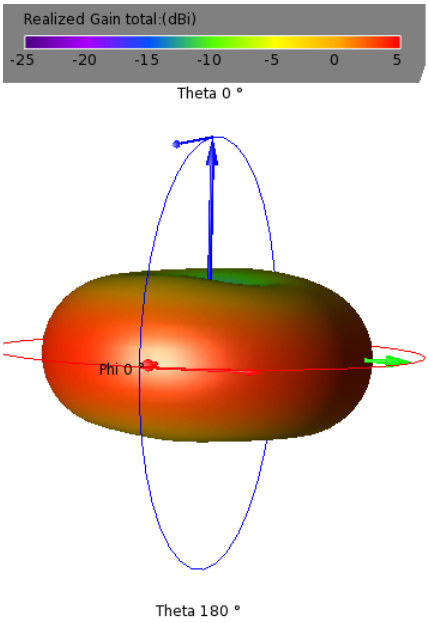

(d) Generation 142

Figure 23. The antenna gain pattern of the most fit individual as of generations 0 (a), 5 (b), and 95 (c) of the single-frequency evolution using the directional gain fitness function.

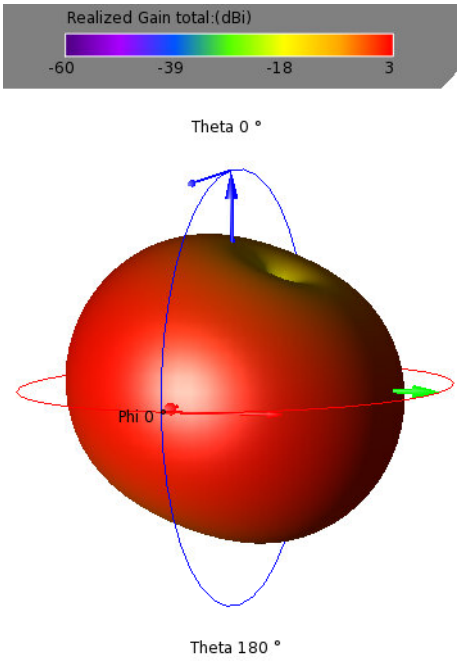

(a) Generation 0
200 MHz

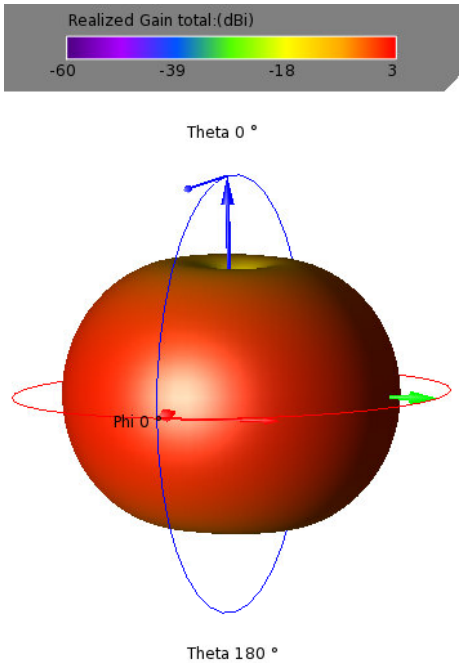

(b) Generation 5
200 MHz

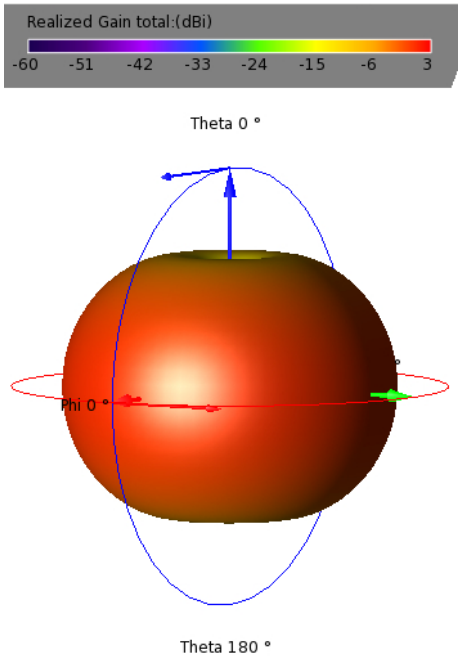

(c) Generation 229
200 MHz

Figure 24. The antenna gain pattern of the most fit individual as of generations 0 (a), 5 (b), and 229 (c) of the broadband evolution using the directional gain fitness function. Shown here are the gain patterns corresponding to a frequency of 200 MHz.

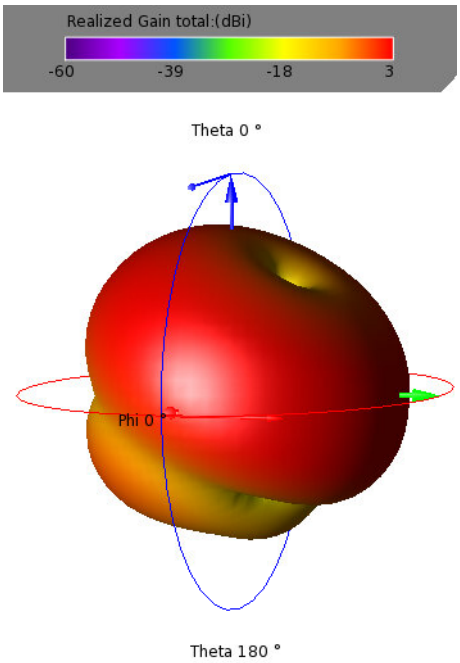

(a) Generation 0
516.73 MHz

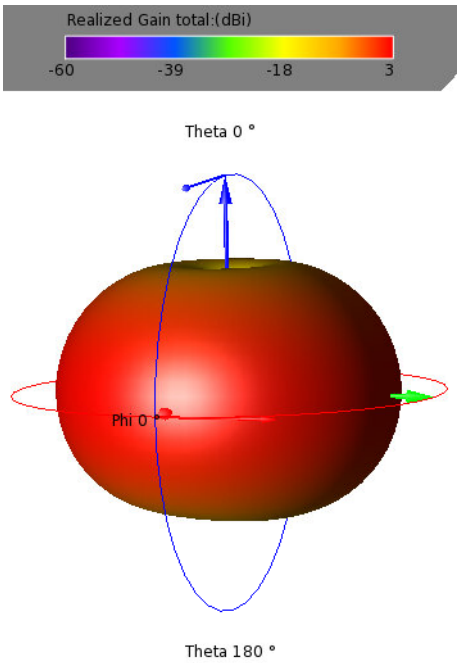

(b) Generation 5
516.73 MHz

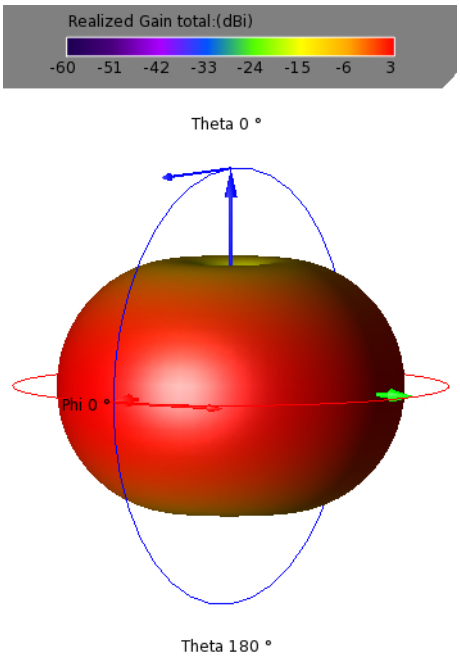

(c) Generation 229
516.73 MHz

Figure 25. The antenna gain pattern of the most fit individual as of generations 0 (a), 5 (b), and 229 (c) of the broadband evolution using the directional gain fitness function. Shown here are the gain patterns corresponding to a frequency of 516.73 MHz.

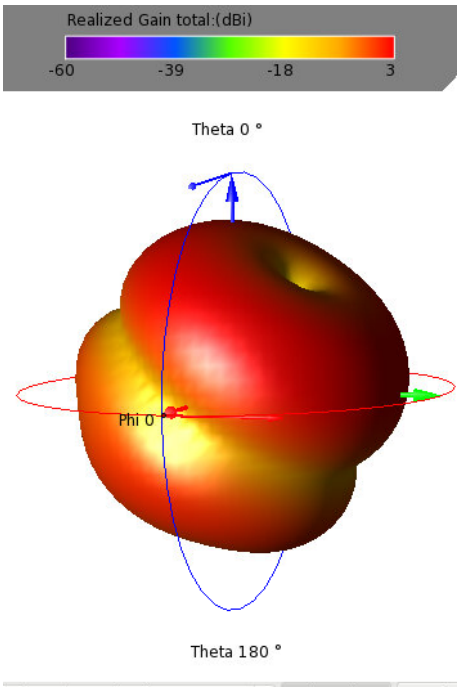

(a) Generation 0
800.1 MHz

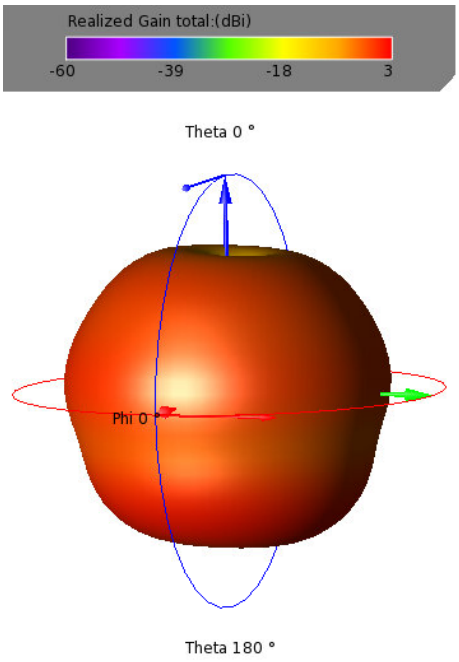

(b) Generation 5
800.1 MHz

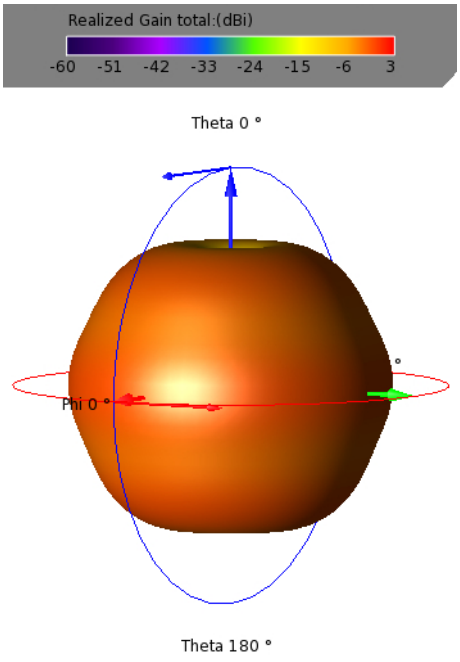

(c) Generation 229
800.1 MHz

Figure 26. The antenna gain pattern of the most fit individual as of generations 0 (a), 5 (b), and 229 (c), of the broadband evolution towards a target radiation pattern (d) using the Euclidean distance-based fitness function. Shown here are the gain patterns corresponding to a frequency of 800.1 MHz.

III. Additional Results

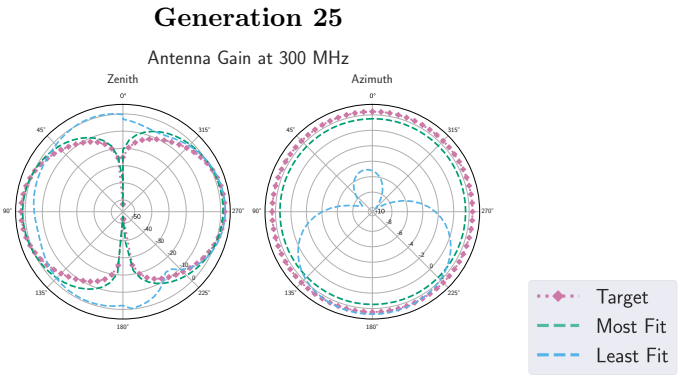

Figure 27. The gain patterns of the most and least fit individual in generation 25 of the single-frequency evolution towards a target radiation pattern using the Euclidean distance-based fitness function. Also overlaid is the gain pattern of the target.

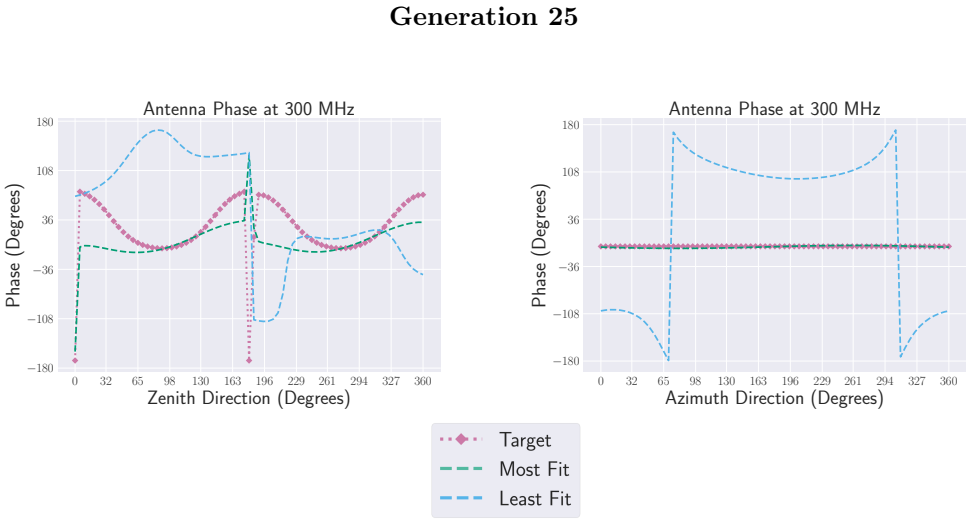

Figure 28. The antenna phase in the zenith and azimuth direction of the most and least fit in generation 25 of the single-frequency evolution towards a target radiation pattern using the Euclidean distance-based fitness function.

Generation 5

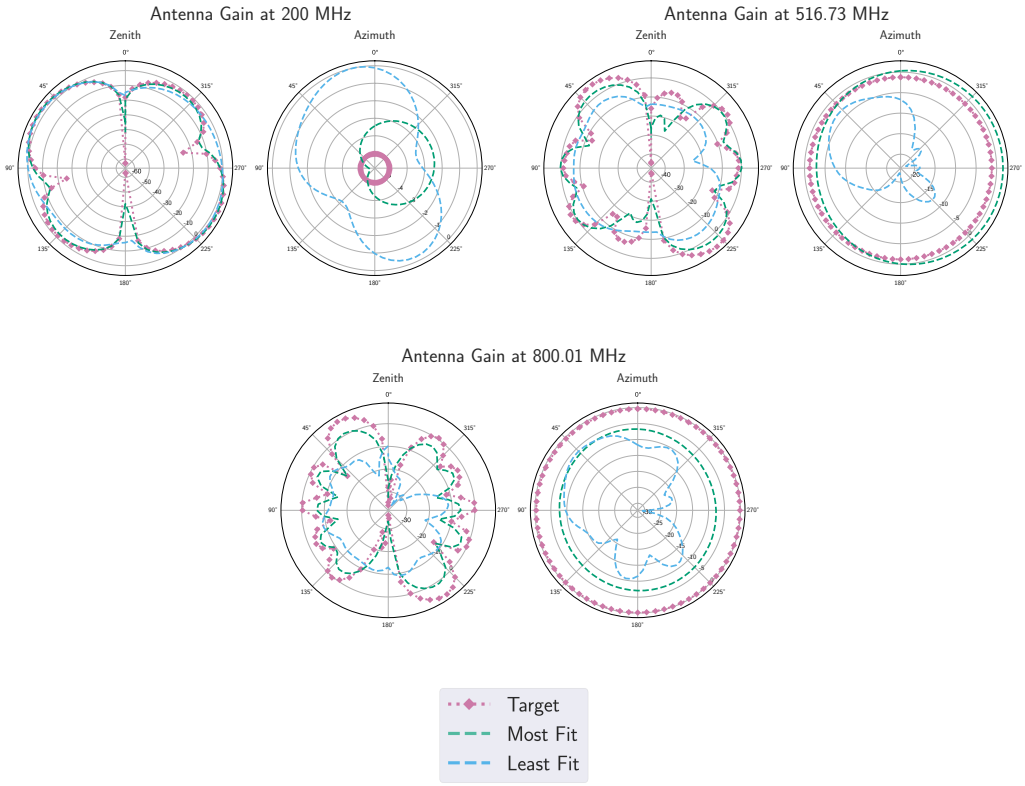

Figure 29. The gain patterns of the most and least fit individuals in generation 5 of the evolution towards a target broadband radiation pattern using the Euclidean distance-based fitness function at three example in-band frequencies: 200 MHz (a), 516.73 MHz (b), and 800.1 MHz (c). Also overlaid on each is the gain pattern of the target at the given frequency.

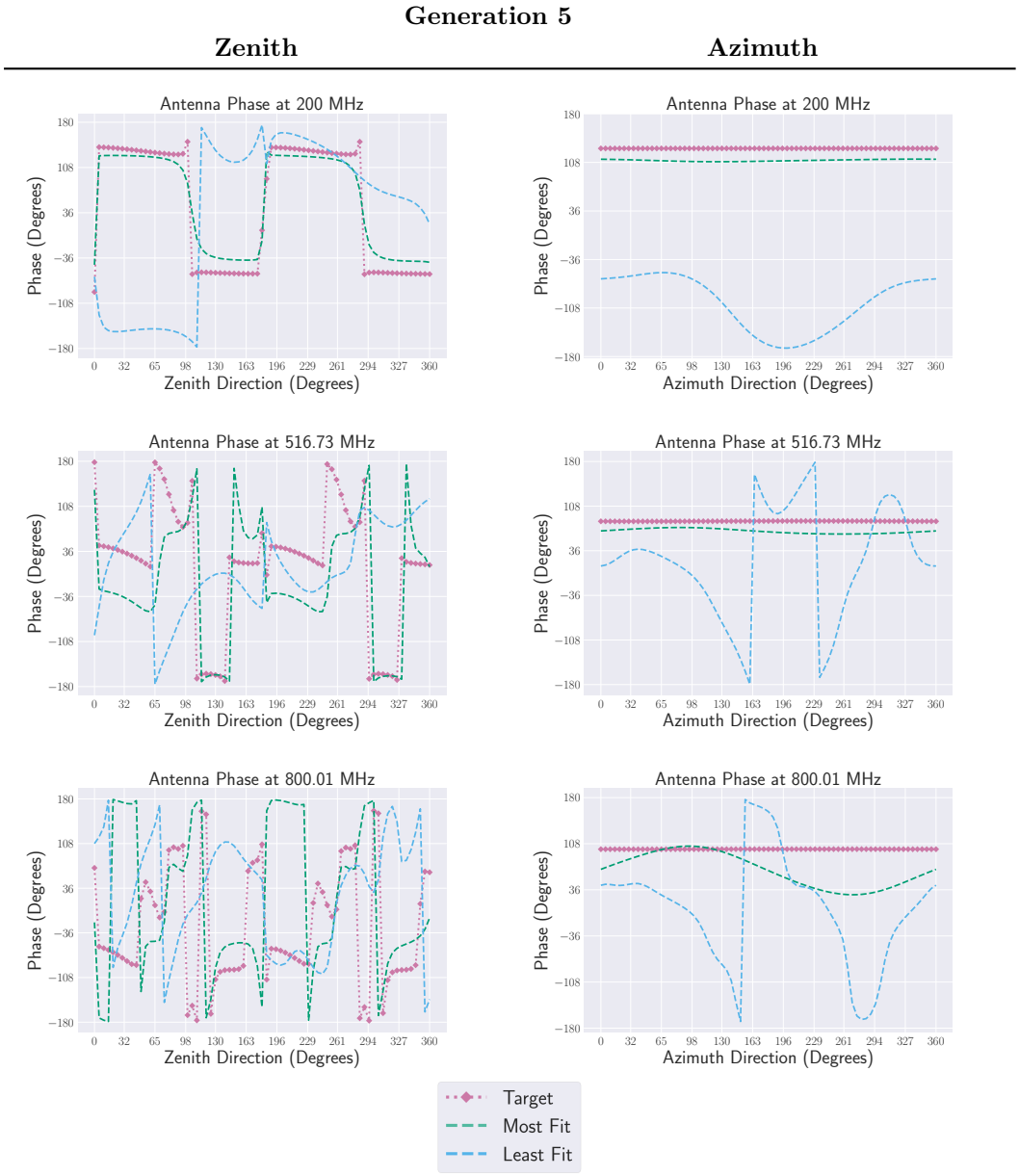

Figure 30. The antenna phase in the zenith and azimuth direction of the most and least fit individual in generation 5 of the evolution towards a target broadband radiation pattern using the Euclidean distance-based fitness function at three example in-band frequencies: 200 MHz (a,b), 516.73 MHz (c,d), and 800.1 MHz (e,f). Also overlaid on each is the phase of the target.

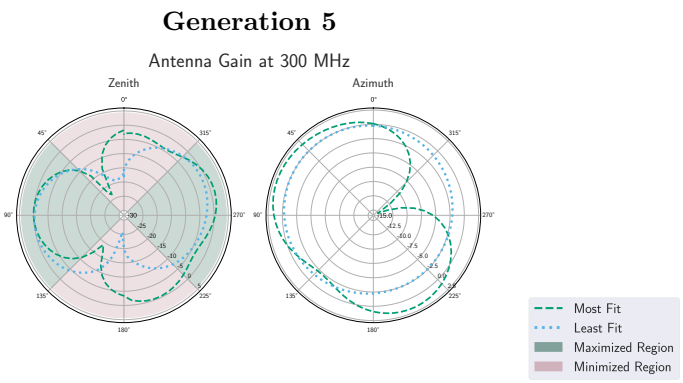

Figure 31. The gain patterns of the most and least fit individual as of generation 5 of the single-frequency evolution using the directional gain fitness function. The regions shaded in green and red represent the angular ranges designated for maximization and minimization, respectively.

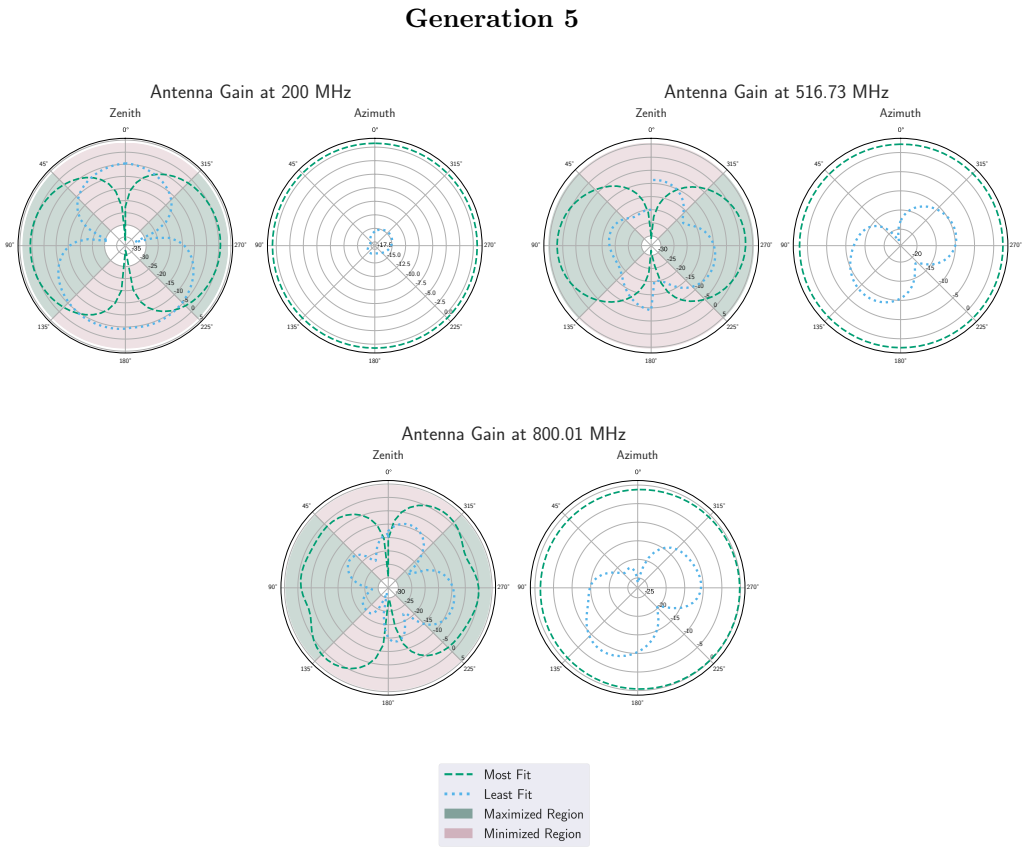

Figure 32. The gain patterns of the most and least fit individuals in generation 5 of the evolution using the directional gain maximization/minimization fitness function at three example in-band frequencies: 200 MHz (a), 516.73 MHz (b), and 800.1 MHz (c). Also overlaid on each is the gain pattern of the target at the given frequency. The regions shaded in green and red represent the angular ranges designated for maximization and minimization, respectively.

IV. Computation Time Per Generation

This section summarizes an analysis conducted on the GA's computation time. Given the large number of generations and individuals that may be necessary to evaluate in order to converge on a solution, it is important to quantify the computation of the algorithm. The study discussed here analyzed the total computation time per generation using data collected during evolutions towards a target broadband radiation pattern using the Euclidean distance fitness function as well as both single-frequency and broadband evolutions using the directional gain fitness function.

A number of factors are expected to influence the typical computation time of a generation, including the number of individuals per generation, number of frequency steps evaluated per individual, overall dimensions and number of shapes making up the individuals, and the number of simulations able to be conducted in parallel. Each of the evolutions that the data presented in this section is drawn from contained 120 individuals per generation, and the other parameters are not expected to deviate significantly between the evolutions towards a target radiation pattern using the Euclidean distance-based fitness function and the directional gain fitness function, with the exception of the number of simulations set to run in parallel. This factor was a user-defined input that was limited by the number of XFdtd software licenses available. For the data presented in this section, the evolutions using the Euclidean distance fitness function utilized the capability to simulate 9 individuals in parallel, while the directional gain evolutions were only capable of simulating 5 individuals in parallel. As a result, the data presented here is grouped accordingly.

Another consideration to note is that the data presented in this section includes the time that jobs spent waiting in the queue of the Ohio Supercomputer Center (OSC), where the antenna simulations were performed. These queue times are an unavoidable component of the overall computation time, and may be inconsistent due to their dependence on resource availability.

The vast majority of computation time necessary to create and evaluate an individual is due to the antenna simulation and queue time. The other stages of the process, including parent selection, application of genetic operators, writing genetic information to file, and modeling the individual, are completed on the order of a few seconds. This is a negligible amount of time relative to the time that it takes to simulate a full generation worth of individuals, which will be seen in the analysis presented here to be on the order of approximately 1 hour or more for a typical generation.

Figure 33 displays a histogram of the computation time per generation from data collected during the evolution towards a target broadband radiation pattern using the Euclidean distance fitness function. The majority of generations completed within approximately 100 minutes. The generations seen to take significantly longer may be attributed to abnormally long queue times due to periods of high traffic at the supercomputing center.

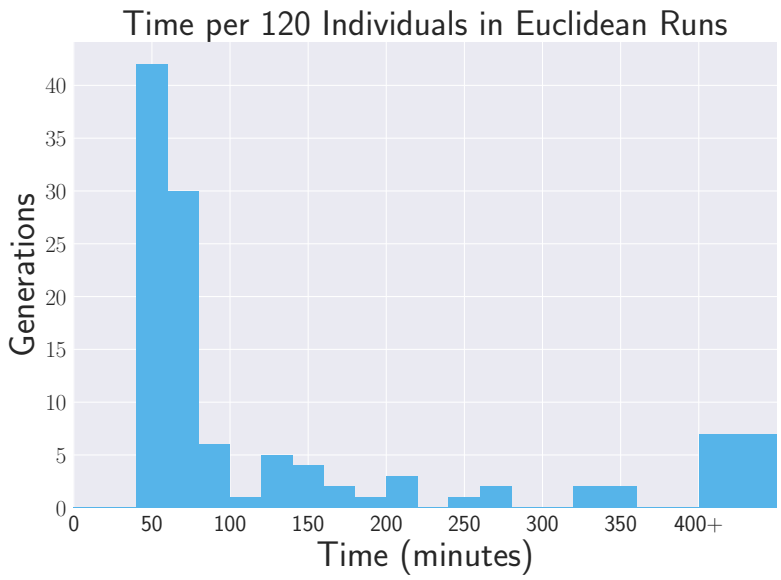

Figure 33. Histogram of the per generation computation time observed during the evolution to a target broadband radiation pattern using the Euclidean distance-based fitness score.

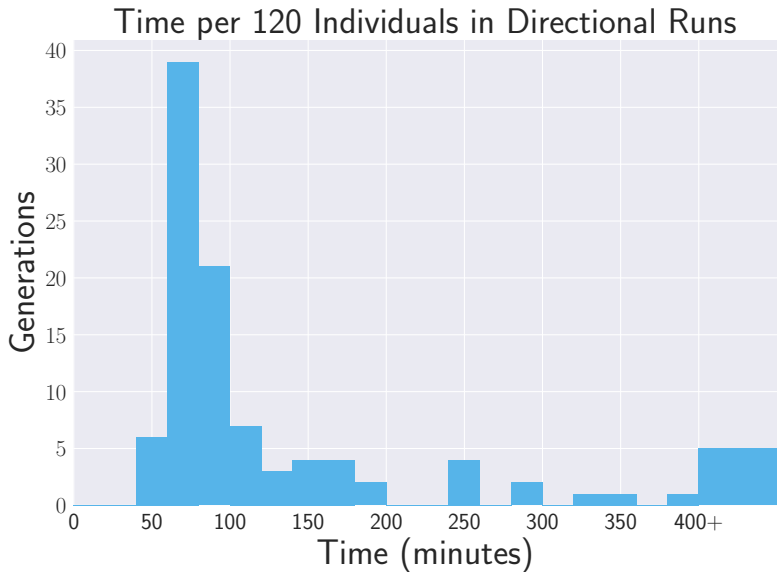

Figure 34. Histogram of the per generation computation time observed during the evolutions using the directional gain fitness score, including both single-frequency and broadband evolutions.

Figure 34 shows a histogram of the computation time per generation from data collected during evolutions using the directional gain fitness function, including data from both single-frequency and broadband evolutions. Most generations still completed within approximately 100 minutes, but the increased computation time due to a lesser amount of parallelization is evident by the increased fraction of generations

with longer durations. The generations seen to take significantly longer may be still be attributed to abnormally long queue times due to periods of high traffic at the supercomputing center.

The results of the analysis presented agree with the expectation that increased parallelization of the simulation of individuals, known to be the most significant contributor to the overall computation time of the evolutions, generally leads to a shorter per generation computation time. Outlier generations significantly longer in duration were observed but are attributed to unavoidable increases in queue time due to limited resources at the computing facilities where the simulations were run.

V. Genetic Algorithm Developments and Performance Studies

Various techniques were explored for reducing total computation time required to converge to a solution by improving the rate of evolution in the GA. These studies were conducted using the direct dictionary comparison fitness function for a shape-to-shape evolution to a log periodic antenna geometry presented in the previous progress report [1].

Figure 35 compares the different steps taken to improve the GA. The baseline result is the evolution presented in the prior report and is shown in the black line. Since this result was obtained, a number of improvements were made to algorithm. Specifically, improvements to the method for recalculating a shape's midpoint after it or the shape that it is connected to has been operated upon and the addition of the side switching regenerative mutation operator significantly increased the probability of individuals finding improved designs. The version of the generational algorithm with these improvements implemented is shown in pink. Implementation of the steady-state algorithm is shown in green and further improves on the rate of convergence. Finally, the fastest version of the GA, shown in yellow, utilized an additional forced diversity constraint and elitism. The forced diversity constraint requires that no child produced be a duplicate of an individual already in the population, and elitism requires that the most fit individual in the population at the current generation be ineligible to be selected for removal.

Additional studies were conducted that allowed the genetic operator probabilities to be changed dynamically in each generation depending on the evolution's current state. This method used reinforcement learning [66] to tune the genetic operator probabilities based on the fitness score growth rate and diversity of the population in each generation. Results of initial tests of the dynamic operator addition to the GA are shown in Figure 36, alongside the performance of various versions of the GA without dynamic operators applied.

The reinforcement learning method for dynamic operators requires model training in order to discover the optimal operator probabilities. This training may either be conducted prior to the start of an evolution and imported, or it may be conducted

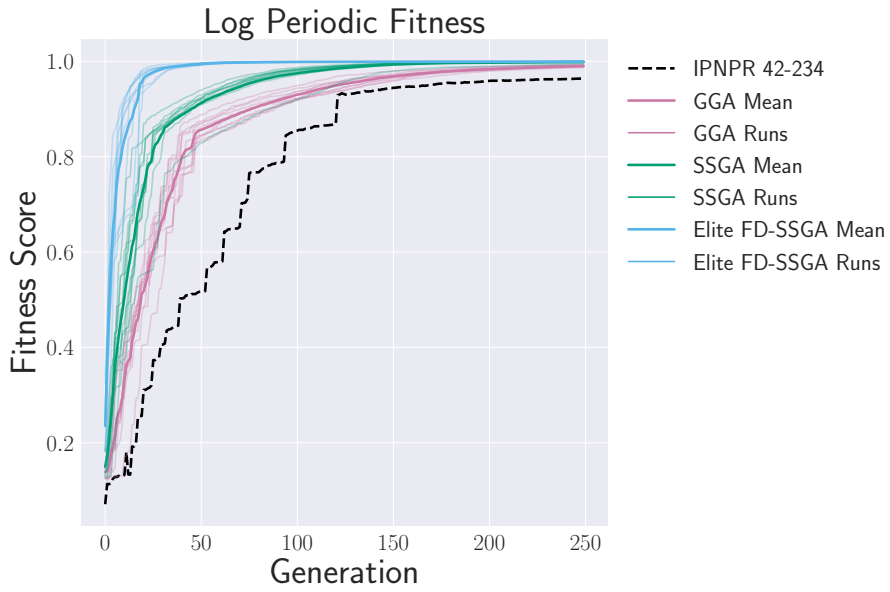

Figure 35. Comparisons of the evolutions using the direct dictionary comparison fitness function for a shape-to-shape evolution to a log periodic antenna geometry [1] using various verisons of the GA. Each result shown is the mean fitness score per generation over 10 trials. Results tested include the original generational GA from the previous progress report in yellow (IPNPR), the updated generational GA in pink (GGA), the steady-state GA in green (SSGA), and the forced diversity steady-state GA in blue (FDSSGA). The lighter lines are individual test runs, and the darker lines are the mean.

using data from the current evolution itself, allowing the algorithm to attempt to learn optimal parameters as it progressed. The pretrained result shown in the orange line on Figure 36 was trained on 200 runs of 250 generations apiece. As seen in Figure 36, it was found that the pretrained test led to faster evolution; however, the existence of ample training data may be restrictive in cases where the per generation run time is long. Further studies of the implementation of dynamic parameter tuning in the GA are planned, including investigation of the impact of allowing various additional parameters to dynamically change throughout an evolution, as well as studies of potential improvements to the reinforcement learning portion of the algorithm.

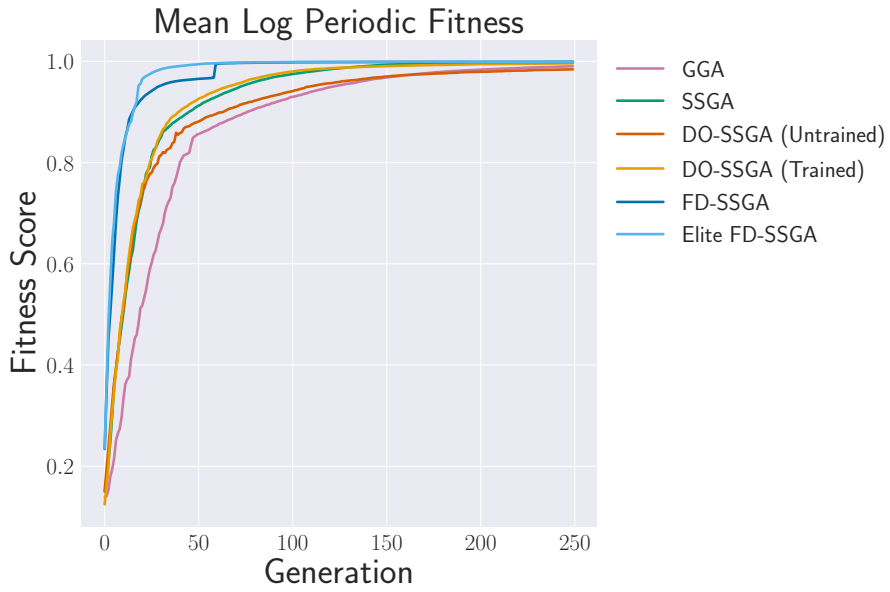

Figure 36. Comparisons of the mean fitness score per generation over 10 trial evolutions for various additions to the GA. Each evolution used the direct dictionary comparison fitness function for a shape-to-shape evolution to a log periodic antenna geometry, as initially described in a previous progress report [1]. Versions of the GA tested include the Generational GA (GGA) in pink, Steady-State GA (SSGA) in green, Steady-State GA with Dynamic Operators without pre-training (DO-SSGA [Untrained]) in red, Steady-State GA with Dynamic Operators with pre-training (DO-SSGA [Trained]) in organge, Forced Diversity Steady-State GA (FD-SSGA) in dark blue, and Forced Diversity Steady-State GA with Elitism (Elite FD-SSGA) in light blue.